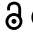



ORIGINAL RESEARCH

 OPEN ACCESS 

## CDK4/6 blockade provides an alternative approach for treatment of mismatch-repair deficient tumors

Inken Salewski<sup>a</sup>, Julia Henne<sup>a</sup>, Leonie Engster<sup>a</sup>, Paula Krone<sup>a</sup>, Bjoern Schneider<sup>b</sup>, Caterina Redwanz<sup>c,d</sup>, Heiko Lemcke<sup>e,f</sup>, Larissa Henze<sup>a</sup>, Christian Junghanss<sup>a</sup>, and Claudia Maletzki<sup>a</sup>

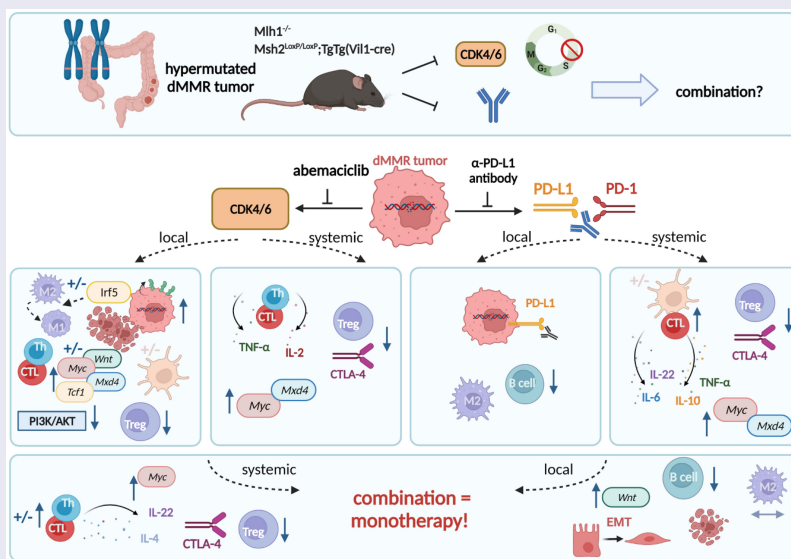
<sup>a</sup>Hematology, Oncology, Palliative Medicine, Rostock University Medical Center, University of Rostock Department of Medicine, Clinic III, Rostock, Germany; <sup>b</sup>Institute of Pathology, Rostock University Medical Center, University of Rostock, Rostock, Germany; <sup>c</sup>Department of Internal Medicine B, Cardiology, University Medicine Greifswald, Germany; <sup>d</sup>Department of Internal Medicine B, Cardiology, University Medicine Greifswald, Greifswald, Germany; DZHK (German Center for Cardiovascular Research), Partner Site Greifswald, Germany; <sup>e</sup>Department of Cardiac Surgery, Reference and Translation Center for Cardiac Stem Cell Therapy (RTC), Rostock University Medical Center, University of Rostock, Rostock, Germany; <sup>f</sup>Faculty of Interdisciplinary Research, Department Life, Light & Matter, Department of Cardiology, Rostock University Medical Center, University of Rostock, Rostock, Germany

### ABSTRACT

Mismatch repair-deficient (dMMR) tumors show a good response toward immune checkpoint inhibitors (ICI), but developing resistance impairs patients' outcomes. Here, we compared the therapeutic potential of an  $\alpha$ -PD-L1 antibody with the CDK4/6 inhibitor abemaciclib in two preclinical mouse models of dMMR cancer, focusing on immune-modulatory effects of either treatment. Abemaciclib monotherapy significantly prolonged overall survival of  $Mlh1^{-/-}$  and  $Msh2^{loxP/loxP;TgTg(Vil1-cre)}$  mice ( $Mlh1^{-/-}$ : 14.5 wks vs. 9.0 wks ( $\alpha$ -PD-L1), and 3.5 wks (control);  $Msh2^{loxP/loxP;TgTg(Vil1-cre)}$ : 11.7 wks vs. 9.6 wks ( $\alpha$ -PD-L1), and 2.0 wks (control)). The combination was not superior to either monotherapy. PET/CT imaging revealed individual response profiles, with best clinical responses seen with abemaciclib mono- and combination therapy. Therapeutic effects were accompanied by increasing numbers of tumor-infiltrating  $CD4^+/CD8^+$  T-cells and lower numbers of M2-macrophages. Levels of T cell exhaustion markers and regulatory T cell counts declined. Expression analysis identified higher numbers of dendritic cells and neutrophils within tumors together with high expression of DNA damage repair genes as part of the global stress response. In  $Mlh1^{-/-}$  tumors, abemaciclib suppressed the PI3K/Akt pathway and led to induction of *Mxd4/Myc*. The immune-modulatory potential of abemaciclib renders this compound ideal for dMMR patients not eligible for ICI treatment.



### ARTICLE HISTORY


Received 4 April 2022  
Revised 22 June 2022  
Accepted 22 June 2022



Two genetic mouse models of spontaneous dMMR-driven tumorigenesis were used in this preclinical therapy trial. Tumor-bearing  $Mlh1^{-/-}$  or  $Msh2^{loxP/loxP;TgTg(Vil1-cre)}$  mice received the CDK4/6 inhibitor abemaciclib, the  $\alpha$ -PD-L1 monoclonal antibody or

a combination of both agents, in which abemaciclib was given as lead-in therapy. Abemaciclib led to an increase of tumor-infiltrating T helper (Th) cells and cytotoxic T cells (CTL), dendritic cells, as well as IRF5-driven polarization of M2 macrophages,

**CONTACT** Claudia Maletzki  [claudia.maletzki@med.uni-rostock.de](mailto:claudia.maletzki@med.uni-rostock.de)  Department of Medicine, Clinic III-Hematology, Oncology, Palliative Care Rostock University Medical Center, Schillingallee 70, Rostock D-18057, Germany

 Supplemental data for this article can be accessed online at <https://doi.org/10.1080/2162402X.2022.2094583>

© 2022 The Author(s). Published with license by Taylor & Francis Group, LLC.

This is an Open Access article distributed under the terms of the Creative Commons Attribution-NonCommercial License (<http://creativecommons.org/licenses/by-nc/4.0/>), which permits unrestricted non-commercial use, distribution, and reproduction in any medium, provided the original work is properly cited.

upregulation of *Mxd4*, and activation of the *Wnt*-signaling. Blood phenotyping revealed reduced levels of T cell exhaustion markers as well as regulatory T cell counts, attributable to Tc-mediated IL-2 secretion. While monotherapy with the  $\alpha$ -PD-L1 monoclonal antibody had slightly different local and systemic effects, the combination approach was not superior to either monotherapy. Notably, most beneficial abemaciclib-mediated immune-modulatory effects were even repealed. Instead, the combination triggered epithelial-mesenchymal transition (EMT), raising caution for CDK-immune-checkpoint-inhibitor combination approaches.  $\pm$ : indicates strain-specific differences.

## Introduction

Mismatch-repair-deficiency (dMMR) arises as a consequence of *MLH1* gene promoter hypermethylation (= sporadic form) or secondary to a germline MMR mutation (= hereditary form). In either case, dMMR is associated with high immunogenicity. Patients harboring dMMR tumors are thus predestined to be treated with immune-checkpoint inhibitors (ICIs). ICIs reactivate exhausted T cells, prevent T cell inhibition, and force T cell-mediated tumor killing.<sup>1</sup> Consequently, Programmed death 1 (PD-1) blockade has emerged as a highly effective treatment strategy and the positive results seen in many patients have contributed to the FDA and EMA approval for first-line therapy of unresectable or metastatic dMMR cancer.<sup>2,3</sup>

Recent data describe superior effects of  $\alpha$ -PD-L1 antibodies compared to  $\alpha$ -PD-1 antibodies in blocking PD-1/PD-L1 signaling.<sup>4</sup> PD-L1 is upregulated in the tumor microenvironment and is found in a large variety of tumors. In recent clinical trials on dMMR patients, the  $\alpha$ -PD-L1 antibody Avelumab has first proven safe<sup>5</sup> and was then compared with standard chemotherapy for treatment of dMMR colorectal cancer patients.<sup>6</sup> Clinical responses up to complete remissions were seen in many cases. Our preclinical data additionally support the use of  $\alpha$ -PD-L1 antibodies either alone or in conjunction with cytostatic drugs and immunotherapy.<sup>7,8</sup> Still, in most cases, resistance mechanisms evolve finally contributing to relapse.<sup>9</sup>

To improve outcomes, ICIs should be combined with other (targeted) agents. A very attractive option is the selective cyclin-dependent kinase 4/6 inhibitor (CDKI) abemaciclib.<sup>10</sup> Abemaciclib stops the cell cycle at G1, induces swollen and dysfunctional lysosomes, and triggers apoptosis/necrosis in tumor cells.<sup>11–13</sup> This CDK4/6 inhibitor is currently approved for treatment of both early and advanced/metastatic breast cancer, however, more immunogenic tumor types, such as dMMR-related cancers, should be considered as well. The rationale for this is based on the increasing body of evidence that abemaciclib stimulates antitumor immune responses by inducing an “inflamed” microenvironment finally contributing to T cell activation and improved T cell function.<sup>14–17</sup> Actually, a recent study reported transformation of CD8<sup>+</sup> T cells into memory cells upon CDK4/6 inhibition to expand the long-term immunity and efficacy of the cancer treatment – an effect frequently seen after ICI treatment.<sup>18</sup> CDK blockade may thus become an interesting option for dMMR patients not eligible

for ICI treatment. The notion that many patients harbor preformed antitumoral immune responses that can be re-activated (or boosted) by immunotherapy additionally argues in favor of using immune-modulating CDKIs for treatment of dMMR-related malignancies.<sup>19–21</sup>

Using the two preclinical *Mlh1*<sup>-/-</sup> and *Msh2*<sup>loxP/loxP;TgTg (Vill-cre)</sup> mouse models of spontaneous tumorigenesis,<sup>22–25</sup> we initiated a proof-of-concept study and compared the efficacy of a murine  $\alpha$ -PD-L1 antibody (clone 6E11) with the CDK4/6 inhibitor abemaciclib either alone or in combination.

We could show that low-dose abemaciclib treatment is as effective as  $\alpha$ -PD-L1 therapy, but its combination is not superior to the respective monotherapy. Hence, we propose abemaciclib monotherapy as a good alternative for treatment of dMMR patients that cannot be treated with ICI.

## Methods

### *In vitro* experiments

#### Cell culture

Two *MLH1*<sup>-/-</sup> tumor cell lines 328 and A7450 T1 M1 were established and characterized in our lab.<sup>25,26</sup> Cell culture was performed in DMEM/Ham's F12 medium, supplemented with 10% FCS (fetal calf serum), 6 mM Glutamine, and antibiotics (all from Biochrom, Berlin, Germany). Treatment was done with selected CDKIs at doses corresponding to IC<sub>30</sub> values: (I) abemaciclib (= abema): 1  $\mu$ M; (II) dinaciclib (= dina): 100 nM; (III) THZ-1: 0.83  $\mu$ M. Doses were validated before *via* dose response curve analyses.

#### Apoptosis/necrosis, cell cycle analysis, and immunogenic cell death

Cells were treated with abema, dina, or THZ-1 for 72 hours, harvested and stained with 0.2  $\mu$ M Yo-Pro 1 iodide (Thermo Scientific, Ex/Em 491/509 nm; blue laser 488 nm, 20 min, RT). Cells were washed and mixed with 7-AAD viability staining solution (250 ng, Biolegend, San Diego, United States) before measurements. For cell cycle analysis, cells were harvested and incubated with ice-cold 70% ethanol over night at  $-20^{\circ}\text{C}$ . 1 mg/ml RNase (Carl Roth, Karlsruhe, Germany) was preheated at  $37^{\circ}\text{C}$  for 90 min. Ethanol fixed cells were washed twice with 2 ml PBS and centrifuged at 300 g for 10 min. Each sample was mixed with 500  $\mu$ l of preheated RNase and incubated for 45 min in the water bath at  $37^{\circ}\text{C}$ . Cells were washed twice with 2 ml PBS and centrifuged at 300 g for 10 min. Cells were resuspended with 400  $\mu$ l propidium iodide (50  $\mu$ g/ml) and incubated for at least 30 min in the fridge covered from light.

For immunogenic cell death assessment, cells were treated with abemaciclib for 48 h and 72 hours. Supernatants were collected and amounts of high-mobility group protein 1 (HMGB1) were measured by ELISA according to the manufacturers' instructions (Abxexa, Cambridge, UK). Cells were harvested and incubated with a polyclonal rabbit CalR primary antibody (1:50; Abgent, San Diego, CA, USA, 30 min,  $4^{\circ}\text{C}$ ), followed by a secondary FITC-labeled antibody (donkey anti

rabbit, 1:50; Biolegend, 30 min, 4°C). Control cells were stained with the secondary FITC-labeled antibody. Measurements were performed on a FACSVerser Cytometer (BD Pharmingen, San Diego, USA). Data analysis was performed using BD FACSuite software (BD Pharmingen).

### Colony formation assay

Five hundred cells/well were seeded in 6-well plates and were allowed to rest overnight. Cells were treated with abema, dina or were left untreated. After 6 days, medium was removed and cells were stained with 500  $\mu$ l 0.2% crystal violet for 10 min on a rocking plate, followed by washing steps. Some cells were allowed to rest with medium for additional 6 days. Then, they were stained the same way with crystal violet. The number of colonies was evaluated using ImageJ-win64.

### Co-culture assay

Tumor cells were harvested and stained with 5  $\mu$ M CMFDA (15 min, 37°C, 5% CO<sub>2</sub>). Twenty-thousand cells/well were seeded in a 24-well plate. After 24 hours, 200,000 blood cells/well, which were lysed with erythrocyte lysis buffer (155 mM NH<sub>4</sub>Cl (MERCK Millipore, Darmstadt, Germany), 10 mM KHCO<sub>3</sub> (MERCK Millipore), and 0.1 mM EDTA (Applichem, Darmstadt, Germany)) were added. Abemaciclib was used at 1  $\mu$ M. After 24 hours, 10  $\mu$ g/ml  $\alpha$ -PD-L1 was added. After additional 48 hours, tumor cells were harvested. To quantify residual tumor cells, fluorescent microsphere beads (1.4  $\times$  10<sup>5</sup> beads/ml, size: 10  $\mu$ m, Polyscience, Hirschberg an der Bergstrasse, Germany) were used. Measurements were performed on a FACSVerser Cytometer (BD Pharmingen). Data analysis was performed using BD FACSuite software (BD Pharmingen).

### Immunofluorescence of cytoskeleton and ROS

The cytoskeleton and formation of reactive oxygen species (ROS) was visualized. Cells were treated twice with 1  $\mu$ M abemaciclib for 72 hours and stained with 7.5  $\mu$ M ROS Brite 670 (AAT Bioquest, CA, USA, 30 min, 37°C) followed by 125 nM Mitolite Green (AAT Bioquest) staining (45 min, 37°C). Cells were fixed with 4% PFA (30 min, RT), washed thrice with PBS and permeabilized with 0.2% TritonX-100 (15 min, RT). Afterward, Phalloidin-iFluor 594 conjugate (AAT Bioquest) dissolved 1:1000 in 1% BSA was added (30 min, RT), followed by three washing steps and 2 min staining with 1.5  $\mu$ g/ml DAPI.

### In vivo experiments

#### Ethical Statement

The German local authority approved all animal experiments: Landesamt für Landwirtschaft, Lebensmittelsicherheit und Fischerei Mecklenburg-Vorpommern (7221.3-1-062/19; -025/20), under the German animal protection law and the EU Guideline 2010/63/EU. Mice were bred in the animal facility of the University Medical Center in Rostock under specific pathogen-free conditions. Mlh1 genotyping was done according to [21] and Msh2 genotyping was done according to.<sup>22,23</sup> During their whole life-time, all animals received enrichment in the form of mouse-igloos (ANT Tierhaltungsbedarf,

Buxtehude, Germany), nesting material (shredded tissue paper, Verbandmittel GmbH, Frankenberg, Deutschland), paper roles (75  $\times$  38 mm, H 0528-151, ssniff-Spezialdiäten GmbH, Soest, Germany), and wooden sticks (40  $\times$  16  $\times$  10 mm, Abedd, Vienna, Austria). During the experiment, mice were kept in type III cages (Zoonlab GmbH, Castrop-Rauxel, Germany) at 12-h dark:light cycle, the temperature of 21  $\pm$  2°C, and relative humidity of 60  $\pm$  20% with food (pellets, 10 mm, ssniff-Spezialdiäten GmbH, Soest, Germany) and tap water *ad libitum*. When mice were subjected to treatment (= time of tumor development), they were given daily-prepared soaked pellets to ensure proper food intake.

### Experimental protocol

Mice with validated gastrointestinal tumor *via* PET/CT were taken into therapy. Mice received abemaciclib (oral gavage, 75 mg/kg body weight (bw), 1x/week, 8 times in total (q1wx8), Mlh1<sup>-/-</sup> n = 7 mice, Msh2<sup>loxP/loxP;TgTg(Vil1-cre)</sup> n = 9 mice) and  $\alpha$ -PD-L1 antibody (i.p., 2.5 mg/kg bw, biweekly), three times in total (q2wx3), Mlh1<sup>-/-</sup> n = 7 mice, Msh2<sup>loxP/loxP;TgTg(Vil1-cre)</sup> n = 10 mice). The  $\alpha$ -PD-L1 antibody, clone 6E11, was kindly provided by Genentech, a subsidiary of Roche, South San Francisco, USA. Mice receiving the combination were given abemaciclib first as lead-in, followed by  $\alpha$ -PD-L1 injection (Mlh1<sup>-/-</sup> n = 7 mice, Msh2<sup>loxP/loxP;TgTg(Vil1-cre)</sup> n = 10 mice). Control mice were left untreated (Mlh1<sup>-/-</sup> n = 6 mice, Msh2<sup>loxP/loxP;TgTg(Vil1-cre)</sup> n = 10 mice) or received the isotype control antibody (i.p. 2.5 mg/kg bw, Mlh1<sup>-/-</sup> n = 7 mice, Msh2<sup>loxP/loxP;TgTg(Vil1-cre)</sup> n = 7 mice). The health status was monitored daily using a score sheet. Reduction of suffering was ensured by applying humane endpoints (weight loss >15%, pain, changes in social behavior). All mice were sacrificed before they became moribund to prevent pain and distress. Mice were sacrificed due to human endpoints (as outlined above + progressive disease, defined by tumor volume >300 mm<sup>3</sup>), followed by removal of blood, spleen, and tumor.

### PET/CT imaging

The tumor size was measured via PET/CT measurements on a small animal PET/CT scanner (Inveon PET/CT, Siemens Medical Solutions, Knoxville, TN, USA) in accordance to a standard protocol as described before.<sup>25</sup> Mice were anesthetized using isoflurane and received FDG intravenously. Evaluation of the images was performed as described before.<sup>8</sup> Treatment outcome determined according to clinical staging as follows: (I) progressive disease (PD) = tumor volume >25% vs. baseline (= day 0); (II) stable disease (SD): tumor volume similar to initial staging ( $\leq$ 25% vs. day 0); (III) partial response (PR): tumor volume 50% lower or more vs. baseline (=day 0). Follow-up was done at day 30 (= short-term) and, in some cases, at ~day 50 (= long-term follow-up).

### Immune phenotyping

Blood was taken routinely from anesthetized mice (retrobulbar venous plexus). Spleen and tumor tissues were dissociated. Single cells were stained with a panel of conjugated monoclonal antibodies (mAb, 0.125  $\mu$ g to 1.5  $\mu$ g each). Zombie NIR™ Fixable Viability Kit by Biolegend (San Diego, United States) staining

was performed following the protocol Zombie NIR™ Fixable Viability Kit by Biolegend, extracellular staining was performed following the protocol BD Horizon Brilliant Stain Buffer (BD Bioscience), followed by lysis and intracellular staining using the protocol of True-Nuclear™ Transcription Factor Buffer Set by Biolegend. Measurements were performed on a spectral flow cytometer (Cytek™ Aurora). For extracellular stainings Gr1 Alexa Fluor700, CD8 FITC, CD4 APC Fire, CD11b BV570, PD-L1 BV421, NK1.1 BV605, CD19 Spark Blue (Biolegend), CD25 PerCP-eFluor710 (ThermoFisher), CD83 BV750, PD-1 BV650 (BD Bioscience) and for intracellular stainings CTLA-4 PE/Cy7, CD3 PerCP, and Foxp3 Alexa Fluor 647 (Biolegend) were used. Data were analyzed using SpectroFlow™ Version 2.2.0.3. and FlowJo™ Version 10.6.1.

### Multiplex cytokine assay

Cytokine levels of the plasma were measured using a multi-analyte flow assay kit following the instructions of the manufacturer (LEGENDplex™, Biolegend). Measurements were performed on a spectral flow cytometer (Cytek™ Aurora). Data were analyzed using the manufacturer's online Software. Absolute plasma cytokine levels are presented [ng/ml].

### Fragment length analysis

Tumor gDNA was isolated using the Wizard Genomic DNA Purification Kit (Promega). An established panel of coding- and non-coding MS marker was evaluated using the fragment length analysis as described before.<sup>27</sup>

### Nanostring targeted gene expression profiling

Tumor RNA was isolated from cryostat sections using the RNeasy Mini Kit (Qiagen). Then, the RNA was analyzed using Nanostring analysis as described before.<sup>8</sup>

### Quantitative real-time PCR

RNA was isolated using the RNeasy Mini Kit (Qiagen). 1 µg mRNA and 50 ng random Hexamer Primer were incubated for 10 min at 70°C. Sample-mixes were completed with 5x RT buffer complete, dNTPs and 200 units reverse. cDNA was synthesized using the PCR cycler 120 min at 45°C and for 10 min at 70°C. 25 ng cDNA was used for quantitative real-time PCR with the SensiFAST Probe Lo-ROX Kit (Bioline, Memphis, Tennessee, USA). Predesigned Taqman gene expression assays were used: 6-FAM-3'BHQ-1 *Mxd4* (Mm00487523\_m1), 6-FAM-3'BHQ-1 *cMyc* (Mm00487804\_m1), 5-VIC-3'BHQ-1 *Agr2* (Mm01291804\_m1), 6-FAM-3'BHQ-1 *Tgfb1* (Mm01178820\_m1), 6-FAM-3'BHQ-1 *Vimentin* (Mm01333430\_m1), 5-VIC-3'BHQ-1 *N-Cadherin* (Mm01162497\_m1), 6-FAM-3'BHQ-1 *Fpr2* (Mm00484464\_s1), 5-VIC-3'BHQ-1 *Csfl* (Mm00432686\_m1), 6-FAM-3'BHQ-1 *Csf2* (Mm01290062\_m1), 5-VIC-3'BHQ-1 *Tcfl1/Pcbd2* (Mm01342270\_m1), and 6-FAM-3'BHQ-1 *Alox5* (Mm01182747\_m1). Self-designed 5-VIC-3'BHQ-1 *GAPDH* was applied as housekeeping gene. Reaction was performed in the light cycler Viiia7 (Applied Biosystems, Foster City, USA) with the following PCR conditions: 95°C for 10 min, 40 cycles of 15 s at 95°C, and 1 min at 60°C. All reactions were run in triplicates. The mRNA levels of target genes were normalized to GAPDH. Reactions were performed in triplicate wells. The expression level

of each sample was considered by calculating  $2^{-\Delta\text{CT}}$  ( $\Delta\text{CT} = \text{Ct}_{\text{target}} - \text{Ct}_{\text{Housekeeping gene}}$ ), followed by  $2^{-\Delta\Delta\text{CT}}$  quantification, taking values of untreated controls as calibrator.

### Immunofluorescence

Cryostat sections of 4 µm were fixed in cold pure methanol for 8 min, air-dried and unspecific binding site blocked (2% BSA, 2 h) followed by staining with Alexa Fluor 488, Alexa Fluor 594 and Alexa Fluor 647 labeled antibodies CD3, CD4, CD8, CD206, F4/80, CD11b, Gr1, PD-L1, PD-1, and Irf5 (Biolegend). Sections were washed and embedded in Roti Mount Fluor Care DAPI (Roth, Karlsruhe). Visualization was performed on a confocal laser scanning microscope (ZEISS Elyra 7 Confocal Laser Microscope, Zeiss, Jena, Germany). The infiltration pattern was quantified. For infiltrating CD3<sup>+</sup>CD4<sup>+</sup> T helper cells and CD3<sup>+</sup>CD8<sup>+</sup> cytotoxic T cells, numbers were counted in 2–3 high power fields (HPFs)/slide. For regulatory granulocytes and tumor-associated macrophages (TAM), the infiltration pattern was semi-quantitatively analyzed using a scoring system. 0 = no; 1 = mild (1–20 cells/HPF); 2 = moderate (21–40 cells/HPF); 3 = strong (>40 cells/HPF).

### Statistics

GraphPad PRISM software, version 8.0.2 (GraphPad Software, San Diego, CA, USA) was used to perform statistical evaluation. All data are presented as mean + SEM. Data are depicted as scatter plots and bar charts, with individual values representing a single value of an individual mouse. Data showing baseline and follow-up are given as dots connected with a line. The value of significance was set to  $p < .05$ . The data were first tested for normality conducting Shapiro-Wilk test. Then, in case of normality, one-way ANOVA (Tukey's multiple comparison) or unpaired T-Test was accomplished or in case of non-parametric data Kruskal-Wallis or U-Test was performed. Kaplan Meyer survival curves were analyzed using the log rank (Mantel Cox) test. In case of blood phenotyping, outliers were eliminated, when they were above or below the average plus/minus two times the standard deviation.

### Dimensionality Reduction Analysis (t-SNE)

Individual fcs files were imported into FlowJo software (version 10.6.1) (FlowJo, Ashland, Oregon). Ten thousand cells per file (six files per treatment group concerning tumor data, and eight files per treatment group concerning blood and spleen data) were randomly selected and merged into one concatenated file. T-SNE algorithm provided by FlowJo software was performed only on gated live cells. The output was a t-SNE map which we show as a dot-plot. The t-SNE dimensions were used on the original gates to create the overlay t-SNE maps.

## Results

### In vitro effects of CDK blockade and a-PD-L1 treatment

Before performing animal experiments, the two murine Mlh1<sup>-/-</sup> tumor cell lines A7450 T1 M1 and 328 were used to evaluate the effects of different CDK inhibitors on cell cycle,



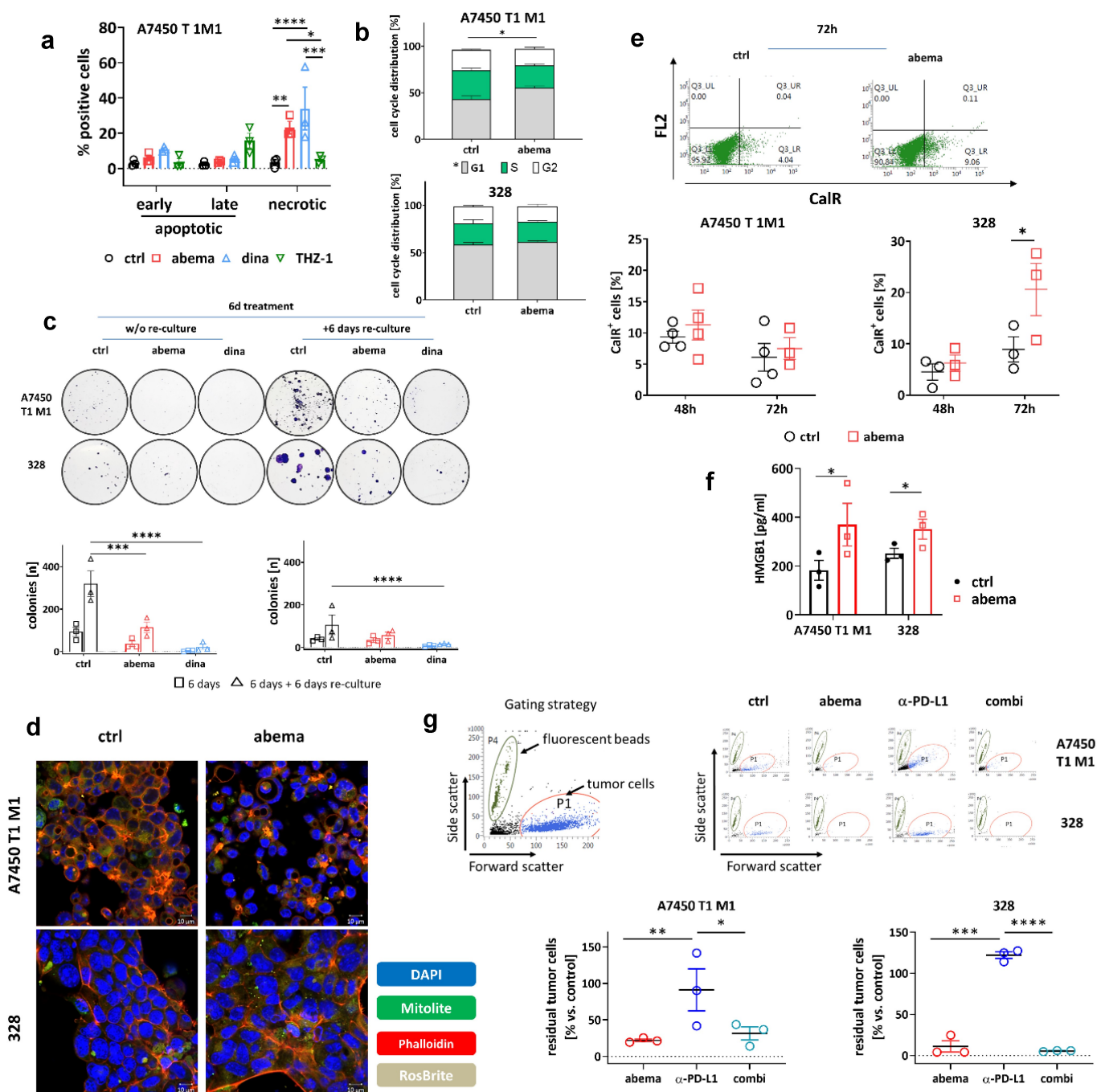


**Figure 1.** *In vitro* analysis on  $Mlh1^{-/-}$  tumor cells. (a) Apoptosis/necrosis quantification.  $Mlh1^{-/-}$  A7450 T1 M1 tumor cells were treated with CDKIs for 72 h and apoptosis/necrosis was quantified from Yo-Pro1/PI-stained cells.  $n = 3$  independent experiments,  $*p < .05$ ;  $**p > .01$ ;  $***p < .001$ ; two-way ANOVA (Tukey's multiple comparisons test). (b) Cell cycle analysis after 48 h of treatment with abemaciclib.  $n = 4$  independent experiments,  $*p < .05$ ; t-test. (c) Colony formation assay after treatment with abemaciclib or dinaciclib. Two experimental conditions were studied: (i) 6 days treatment and direct analysis and (ii) 6 days treatment + 6 days re-culture without (w/o) treatment (= reconvalescence). Thereafter, colonies were counted using ImageJ software.  $n = 3$  independent experiments,  $*p < .05$ ;  $***p < .001$ ;  $****p < .0001$ ; two-way ANOVA (Tukey's multiple comparisons test). (d) Detection of ROS (RosBrite), cytoskeleton (Phalloidin) and mitochondria (mitolite) after 48 h of treatment with abemaciclib. Representative images are shown out of  $n = 3$  independent experiments. Read out was done with the ZEISS Elyra 7 Confocal Laser Microscope (Zeiss). Original magnification 400 x. (e) Flow cytometric measurement of CalR-positive cells after 48 h and 72 h of treatment.  $n = 3-4$  independent experiments. (f) HMGB1 secretion after 72 h of treatment. HMGB1 levels were determined from supernatants of  $Mlh1^{-/-}$  tumor cells. Control cells were left untreated. Experiments were repeated three times each of them performed in duplicates.  $*p < .05$ . (g) Co-culture of tumor and immune cells. Tumor and immune cells were simultaneously treated for  $1 \times 72$  h with abemaciclib,  $\alpha$ -PD-L1 antibody or a combination. The effector to target ratio was 1:10. Residual tumor cells were counted by adding fluorescent beads. Read out was done via flow cytometry. Representative dot plots of tumor cells treated with immune cells and drugs are shown.  $n = 3$  independent experiments,  $*p < .05$ ;  $**p < .01$ ,  $***p < .001$ ;  $****p < .0001$ , One-way ANOVA (Tukey's multiple comparisons test). (a-g) All data are given as mean  $\pm$  SEM. Doses used in each experiment are as follows: abemaciclib: 1  $\mu$ M, dinaciclib: 0.1  $\mu$ M, THZ-1: 0.83  $\mu$ M;  $\alpha$ -PD-L1 antibody: 10  $\mu$ g/ml.

proliferation, morphology, and immunogenic cell death (Figure 1a–e). In some experiments, the  $\alpha$ -PD-L1 antibody was added and combinations were tested (Figure 1e, f).

The selective CDK4/6 inhibitor abemaciclib and the global CDK1/2/5/9 inhibitor dinaciclib significantly increased the number of necrotic cells. By contrast, selective CDK7 inhibition by THZ-1 did not induce significant cell death (Figure 1a). Abemaciclib led to a G1-arrest in A7450 T1 M1 cells, whereas in 328, the number of cells in the G1-phase was slightly reduced (Figure 1b). Upon dinaciclib, the number of cells in S-phase increased in both cell lines. Using a classical colony formation assay, the number of A7450 T1 M1 colonies was reduced after abemaciclib and even more pronounced after dinaciclib treatment (Figure 1c), both after 6 days of treatment and significantly after additional 6 days of rest.

Then, we focused on abemaciclib for further studies. This agent affected the cytoskeleton and reduced mitochondria of A7450 T1 M1 cells. By contrast, reactive oxygen species remained unchanged (Figure 1d). In 328, we did not observe such strong changes in colony formation, cytoskeleton, and mitochondria, but reactive oxygen species were slightly decreased. The amount of CalR<sup>+</sup> A7450 T1 M1 cells was comparable to controls, while in 328 cells, surface-bound CalR was more abundant after 72 hours of abemaciclib treatment (Figure 1e). Likewise, HMGB1 levels significantly increased, indicative for induction of immunogenic cell death (figure 1f).

In a subsequent co-culture assay, the impact of immune cells on the tumor cell viability was investigated (Figure 1g). Abemaciclib alone and its combination with  $\alpha$ -PD-L1 reduced tumor cell numbers significantly.

Taken together, CDKs have individual effects on MMR-D tumor cells. The immune-stimulating potential of abemaciclib may interact with immune-checkpoint blockade. To address this further, we initiated a proof-of-concept *in vivo* therapy trial.

### **Prolonged survival and effective tumor growth control under mono- and combination therapy**

We included two preclinical mouse models of spontaneous, dMMR-driven tumorigenesis. Mlh1<sup>-/-</sup> mice harbor a constitutional knock out, whereas in Msh2<sup>loxP/loxP;TgTg(Vil1-cre)</sup> mice, a conditional knock out in the gut is the driver for tumor formation.<sup>23,25,28</sup> These mice share some features commonly related to dMMR, such as a high tumor mutational burden, and an inflamed tumor microenvironment. However, the infiltration pattern of specific immunological subtypes differs, nicely reflecting the clinical presentation of dMMR-related cancer (Table 1). Hence, these models are ideal tools for preclinical response analysis.

Treatment with abemaciclib was given weekly at a dose of 75 mg/kg bw because of its therapeutic activity *in vitro* even after drug removal and its capacity to stimulate the immune system.<sup>14,16,18,29</sup> The treatment schedule of the  $\alpha$ -PD-L1 antibody was adopted to our previous study<sup>8</sup> with a biweekly application route at a dose of 2.5 mg/kg bw. Tumor growth was monitored in both mouse models before and after treatment using<sup>18</sup>F-FDG PET/CT (please see Figure 2a for experimental protocol).

Monotherapy with  $\alpha$ -PD-L1 and abemaciclib reduced tumor sizes in Mlh1<sup>-/-</sup> mice (Figure 2b,  $p < .05$  abemaciclib vs. control). The combination approach, in which abemaciclib was given as lead-in, had comparable effects. Control and isotype-treated mice showed the expected increased tumor sizes. By dissecting the response rates in more detail, we identified partial response or stable disease in all mice receiving abemaciclib or the combination. By contrast, partial response was only seen in one case after  $\alpha$ -PD-L1 monotherapy and in neither mouse of the control groups (Figure 2b, d).

The response pattern of Msh2<sup>loxP/loxP;TgTg(Vil1-cre)</sup> mice was comparable to those of Mlh1<sup>-/-</sup> mice (Figure 2c, e). Short-term follow-up was available for all mice receiving treatment, whereas, in the controls, only half of them underwent follow-up because of disease progression. 66.0% of mice had partial response or stable disease under abemaciclib and 44.4% mice under combination therapy (vs. 37.5% in the  $\alpha$ -PD-L1 and neither in the control groups).

Long-term follow-up (> day 50) principally confirmed the good response toward abemaciclib in both mouse strains (figure 2f, g). Fifty percent of mice showed partial response. The  $\alpha$ -PD-L1 primarily induced stable disease. The response pattern toward monotherapy was not confirmed in the combination. Here, 50% of Mlh1<sup>-/-</sup> mice had partial response, while all Msh2<sup>loxP/loxP;TgTg(Vil1-cre)</sup> mice suffered from progressive disease (figure 2f, g).

All three therapies significantly improved the outcome in both mouse strains (Mlh1<sup>-/-</sup>:  $p < .001$ , Msh2<sup>loxP/loxP;TgTg(Vil1-cre)</sup>  $p < .001$ , Figure 2h,i). Median overall survival of Mlh1<sup>-/-</sup> mice receiving abemaciclib alone was 14.5 weeks and thus even better than under  $\alpha$ -PD-L1 monotherapy (9.0 weeks). In Msh2<sup>loxP/loxP;TgTg(Vil1-cre)</sup> mice, both monotherapies yielded comparable outcomes (abemaciclib vs.  $\alpha$ -PD-L1: 11.7 vs. 9.6 wks). Still, the combination was not superior to either monotherapy.

To check whether potential hepatotoxic effects of the applied regimens may account for treatment failure in the combination group, routine histology was done. This analysis revealed massive focal lymphocytic and granulocytic infiltration in livers from mice treated with abemaciclib or  $\alpha$ -PD-L1 monotherapy (supplementary Figure S1, 63x magnification of single lymphocytes and granulocytes in the left corner, infiltrates are marked with a black arrow). While this was a likely result of the systemic immune stimulation, such strong lymphocytic infiltration was only partially preserved in the combination treatment, with single necrotic areas arising (black arrow). We conclude antagonistic instead of synergistic effects of combined CDK4/6 – immune-checkpoint blockade in these two preclinical dMMR tumor models.

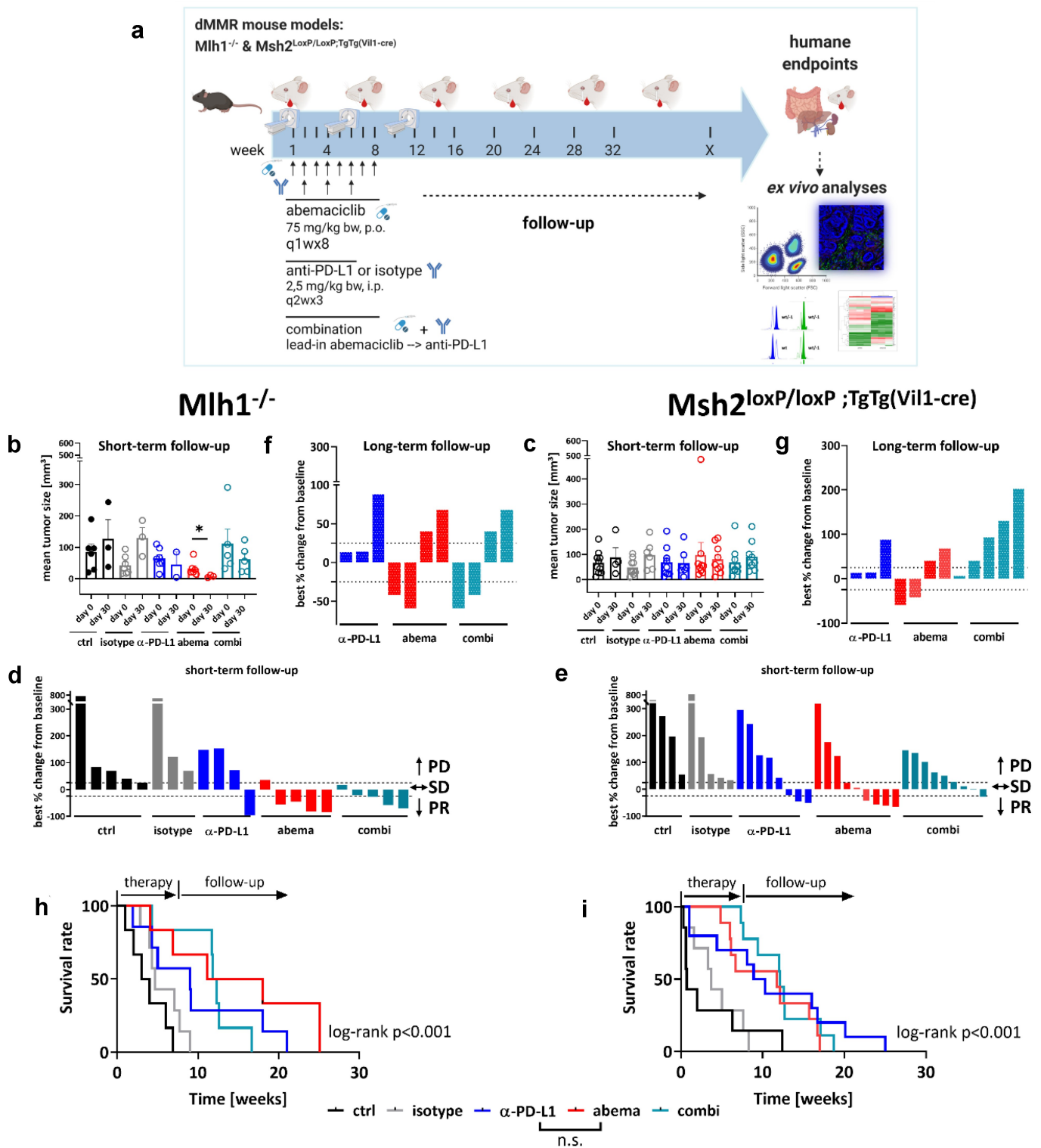
### **Treatment-related immunological changes in the periphery and spleen**

To get an idea on the mechanisms underlying this individual response pattern *in vivo*, plasma samples were taken from control and treatment groups at baseline (=before treatment) and after therapy (= experimental endpoint). A panel of cytokine markers was studied to cover the most relevant Th1 and Th2-specific cytokines and to track the changes under therapy (Figure 3).

**Table 1.** Overview on similarities and disparities between *Mlh1*<sup>-/-</sup> and *Msh2*<sup>loxP/loxP Villin Cre</sup> mice

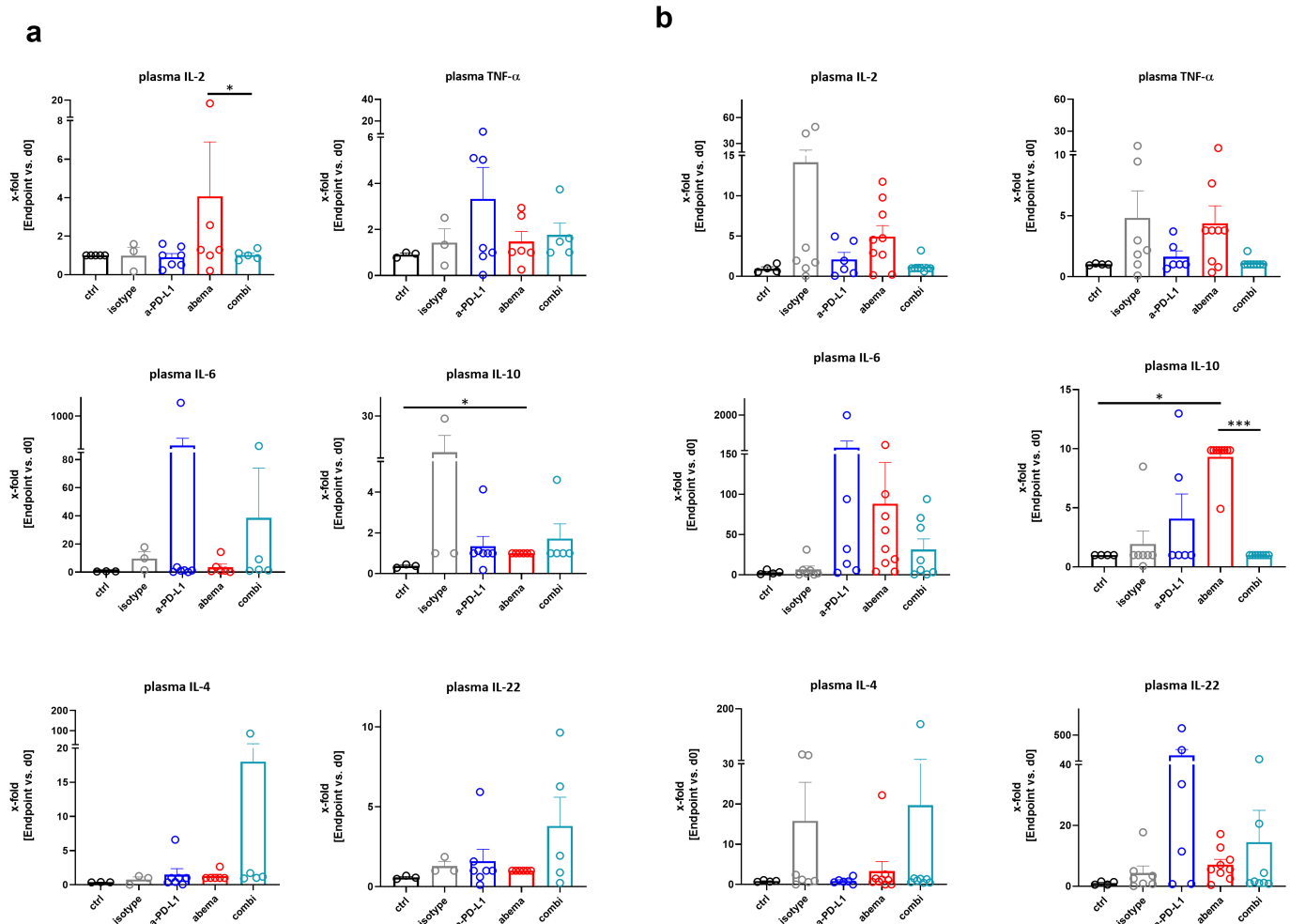
Characteristic	Mlh1 <sup>-/-</sup>		Msh2 <sup>loxP/loxP Villin Cre</sup>	
	Mouse	Human	Mouse strain	C57Bl/6
Strain specificity and model establishment			Spontaneous tumor formation	Constitutional
Clinicopathological characteristics	Human	Human	Frequency of the underlying MMR defect in human	Yes ~35 %
	Mouse	Mouse	Human disease counterpart Human lifetime risk of tumorigenesis Murine mean age of onset Tumor penetrance Tumor spectrum	Lynch syndrome and constitutional mismatch repair deficiency ♂ : 27 – 74 % ♀ : 22 – 53 % 26 weeks (lymphoma), 35 weeks (GIT) High, >90 % LS-associated tumors ≥ hematological malignancies (lymphoma) > others (skin)
Tumor microenvironment	Mouse		Manifestation Metastatic spread MHC class I expression MSI in mononucleotide repeats MSI in coding mononucleotide repeats Cytotoxic T-cells T helper cells MDSC TAM PD-L1	Jejunum No 100% positive High High Moderate Low Moderate Moderate Moderate Good Missing
Treatment response towards			Immune checkpoint inhibition (α-PD-L1) CDK4/6 inhibition Combined ICI/CDKI Circulation	Poor > moderate Good Missing IL-2 and TNF-α secretion; Treg, B cells ; MDSC
Immunological effects upon CDKI treatment			Spleen Tumor DNA Damage repair PI3K-Akt Wnt signaling Epigenetic regulation JAK-STAT signaling EMT	Missing IL-2, TNF-α, IL-6 secretion, IL-10 secretion; B cells, Treg, CTLA-4 <sup>+</sup> cells ; MDSC Treg, CTLA-4 <sup>+</sup> cells <i>Agr2</i> ; B cells; Treg ; TAM Unaffected Unaffected Unaffected Induced Induced Not induced
Pathway alteration upon CDKI treatment				

TIL - tumor-infiltrating lymphocytes; GIT - gastrointestinal tumor; MDSC - myeloid-derived suppressor cells; TAM - tumor-associated macrophages; CDK - cyclin-dependent kinase; CDKI - cyclin-dependent kinase inhibitor; ICI - immune checkpoint inhibition; DC - dendritic cells; EMT - epithelial-mesenchymal transition.



**Figure 2. Treatment schedule, longitudinal <sup>18</sup>F-FDG PET/CT imaging in vivo and overall survival of Mlh1<sup>-/-</sup> and Msh2<sup>LoxP/LoxP;TgTg(Vil1-cre)</sup> mice.** (a) Experimental protocol. Mice with gastrointestinal tumors were conducted to mono- or combination therapy. Abemaciclib: 1x/week, 8 times in total (q1wx8); α-PD-L1: biweekly, 3 times in total (q2wx3); combination: abemaciclib first (=lead-in), followed by α-PD-L1 injection. (b – g) Baseline and follow-up PET/CT imaging of individual mice. (b, c) Data are presented in column (each dot stands for an individual mouse). (d, e, f, g) Data are presented as best % change from baseline according to clinical definitions and depicted for each individual mouse either after short-term (day 30) (d, e) or long-term follow-up (~day 50) (f, g); PD – progressive disease (tumor volume > 25% vs. baseline), SD – stable disease (tumor volume similar to initial staging (≤ 25% vs. day 0); PR – partial response (tumor volume 50% lower or more vs. baseline). (h, i) Kaplan-Meier survival curve. Mlh1<sup>-/-</sup>: isotype vs. α-PD-L1: *p* < .05; control vs. abemaciclib: *p* < .01; control vs. combination: *p* < .01; ctrl: *n* = 6, isotype: *n* = 7, α-PD-L1 *n* = 7, abemaciclib: *n* = 6, combination *n* = 6. Msh2<sup>LoxP/LoxP; Vil1Cre</sup>: isotype vs. α-PD-L1: *p* < .05; control vs. abemaciclib: *p* < .01; control vs. combination: *p* < .001. ctrl: *n* = 10, isotype: *n* = 7, α-PD-L1 *n* = 10, abemaciclib: *n* = 9, combination *n* = 9. Log-rank analysis (Mantel Cox).



**Mlh1<sup>-/-</sup>****Msh2<sup>loxP/loxP</sup>;TgTg(Vil1-cre)**

**Figure 3. Cytokine levels of plasma from Mlh1<sup>-/-</sup> and Msh2<sup>loxP/loxP</sup>;TgTg(Vil1-cre) mice.** (a) Mlh1<sup>-/-</sup> and (b) Msh2<sup>loxP/loxP</sup>;TgTg(Vil1-cre) Plasma samples were collected before treatment (= baseline) and at the experimental endpoint. Cytokine levels were determined as described in material and methods. Given is the x-fold change of the indicated marker in comparison to day 0 (= baseline). Mlh1<sup>-/-</sup>: ctrl: n = 3, isotype: n = 3, α-PD-L1 n = 7, abemaciclib: n = 6, combination n = 5. Msh2<sup>loxP/loxP</sup> Vill1Cre: ctrl: n = 4, isotype: n = 7, α-PD-L1 n = 6, abemaciclib: n = 9, combination n = 8. \**p* < .05; \*\*\**p* < .001, Kruskal-Wallis test (Dunn's multiple comparisons test). (a-b) All data are given as mean + SEM.

Monotherapy with abemaciclib induced IL-2 secretion in Mlh1<sup>-/-</sup> mice, while the α-PD-L1 antibody evoked TNF-α and IL-6 release (Figure 3a). However, this did not reach statistical significance. In mice receiving the combination, we detected increased levels of IL-4 and IL-22. IL-10 was not altered under therapy. In Msh2<sup>loxP/loxP</sup>;TgTg(Vil1-cre) mice, IL-2, TNF-α, IL-6, and IL-10 level were higher under abemaciclib treatment (Figure 3b). The α-PD-L1 monotherapy led to a strong increase of IL-6 and IL-22 (Figure 3b and supplementary Figure S2A). The combination triggered the release of IL-6 and IL-22 secretion, but not to a degree comparable to either monotherapy.

While these data already hinted toward individual effects on the immune system, we then focused on blood phenotyping to dissect the immunological changes in detail. Therefore, a panel of specific antibodies was used to quantify numbers of circulating T cell subpopulations (including exhausted and activated T cells), NK cells, B cells, and myeloid-derived suppressor cells (MDSC) via flow cytometry (Figure 4, supplementary Figure S2B, C).

This analysis identified decreased levels of regulatory T cells (Tregs) in Mlh1<sup>-/-</sup> and Msh2<sup>loxP/loxP</sup>;TgTg(Vil1-cre) mice and in all treatment groups (Figure 4a, b). In Mlh1<sup>-/-</sup> mice, CTLA-4<sup>+</sup> cells showed only reduced levels under α-PD-L1 mono- and combination therapy (Figure 4c). This was additionally seen for CD19<sup>+</sup> cells (supplementary Figure S2B). In contrast, the percentage of MDSCs was highly increased in the combination. NK cells remained unchanged (supplementary Figure S2B).

Comparable effects on Tregs and exhaustion markers were evident in Msh2<sup>loxP/loxP</sup>;TgTg(Vil1-cre) mice (Figure 4b, d). Exemplarily shown for CTLA-4<sup>+</sup> T cells, the percentage of circulating cells was reduced under all three treatments (Figure 4d). Notably, both monotherapies reduced the amounts of exhausted PD-1<sup>+</sup> T cells (not shown). The MDSCs, B cells, and NK cells showed diverging results, with the former showing treatment-related increases (supplementary Figure S2C).

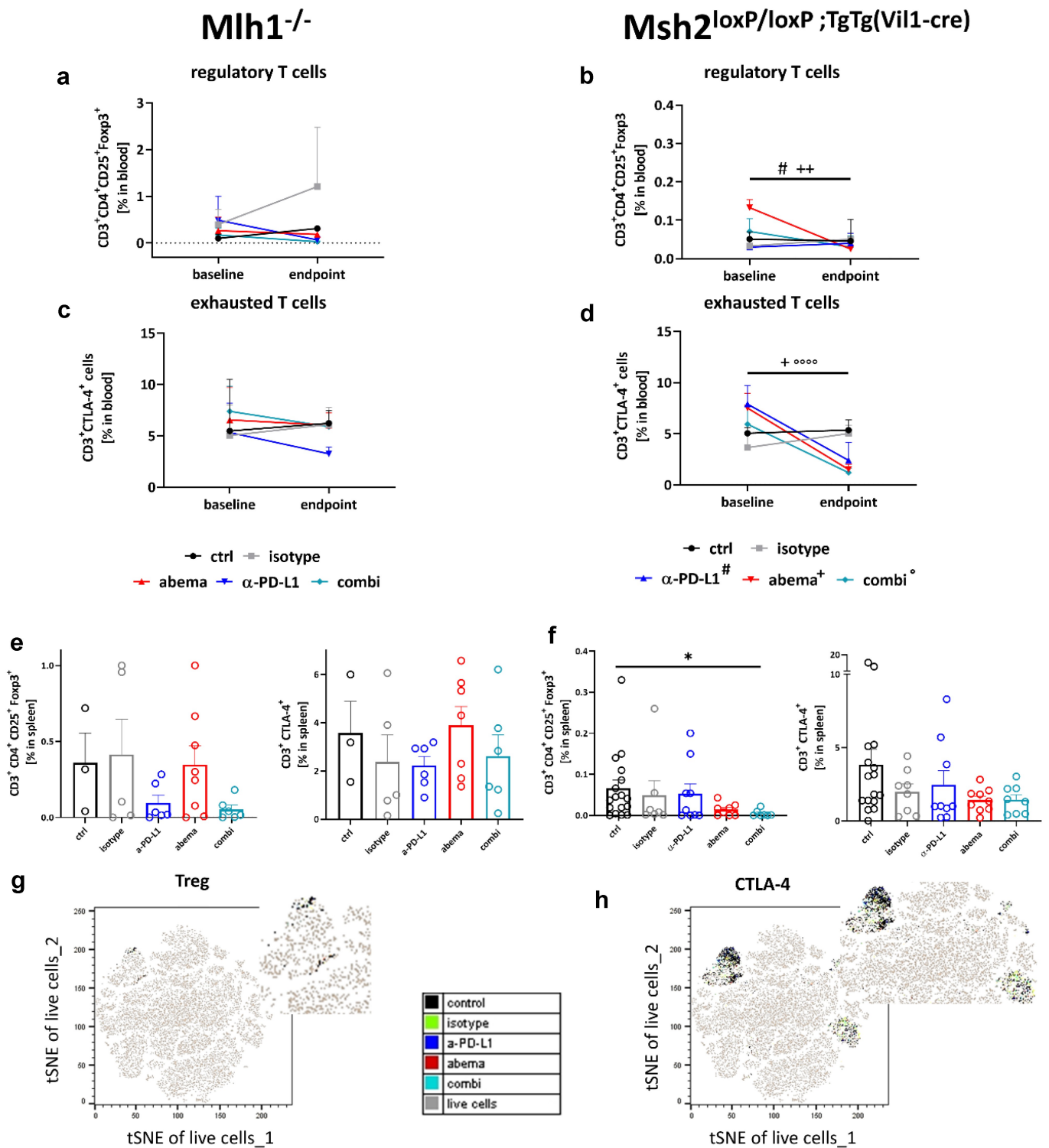


**Figure 4. Spectral flow cytometry of peripheral blood and spleens from *Mlh1*<sup>-/-</sup> and *Msh2*<sup>loxP/loxP;TgTg(Vil1-cre)</sup> mice.** (a – d) Blood phenotyping. Given is the number of % immune cells before treatment (= baseline) and at the experimental endpoint resulting from 100,000 events measured on a flow cytometer. *Mlh1*<sup>-/-</sup> n = 3–8 mice/group, *Msh2*<sup>loxP/loxP;TgTg(Vil1-cre)</sup> n = 7–9 mice/group. \**p* < .05 endpoint vs. day 0 α-PD-L1; +*p* < .05 endpoint vs. day 0 abemaciclib; ++*p* < .01 endpoint vs. day 0 abemaciclib, \*\*\*\**p* < .0001 endpoint vs. day 0 combination. Kruskal-Wallis test (Dunn’s multiple comparisons test). (e – h) Spleen phenotyping. Given is the number of % immune cells at the experimental endpoint resulting from 100,000 events measured on a flow cytometer. \**p* < .05; Kruskal-Wallis test (Dunn’s multiple comparisons test). (g, h) tSNE plots showing single T cell subpopulations of spleens from *Msh2*<sup>loxP/loxP;TgTg(Vil1-cre)</sup> mice. The expression profile of the exhaustion marker CTLA-4 as well as Tregs were illustrated for the treatment and control groups, respectively.

Next, we focused on splenic T cells (Figure 4e, f). In *Mlh1*<sup>-/-</sup> mice, Tregs were only reduced under α-PD-L1 mono – and combination treatment (Figure 4e). Abemaciclib alone did not

change the amount of Tregs. Also, exhausted T cells remained unchanged under therapy. In *Msh2*<sup>loxP/loxP;TgTg(Vil1-cre)</sup> mice, abemaciclib alone and in combination with α-PD-L1 reduced

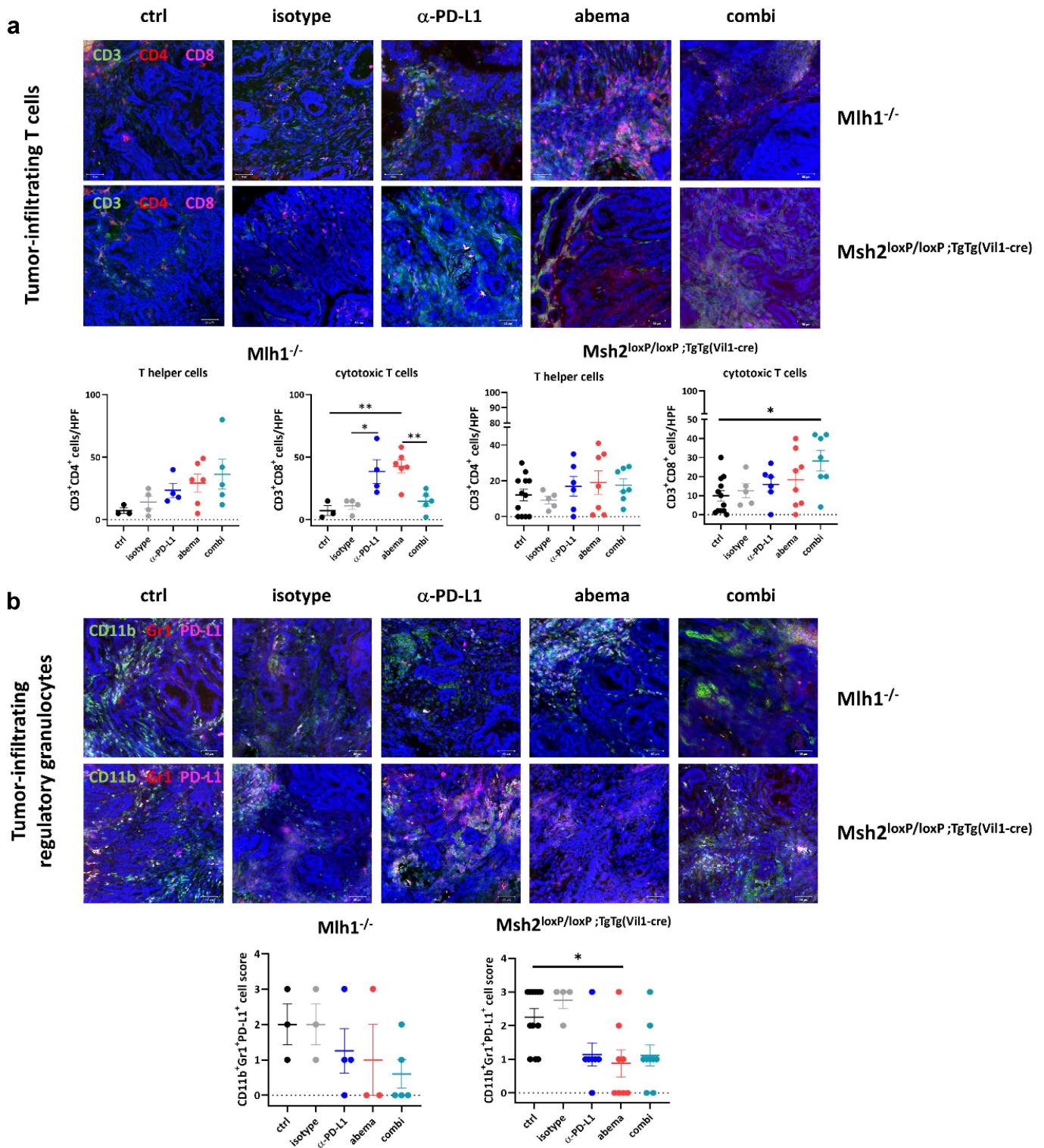


**Figure 5. Immunofluorescence of tumor specimens from Mlh1<sup>-/-</sup> and Msh2<sup>loxP/loxP</sup>;TgTg(Vil1-cre) mice.** Residual tumor slides were fixed, stained and embedded. Confocal laser scanning microscopy was done on a Zeiss Elyra 7 microscope. The infiltration pattern of T cells, regulatory and tumor-associated macrophages differed between individual treatment groups. In most cases, the differences reached statistical significance. Upper panel: representative images of tumor slides; lower panel: quantitative analysis of tumor-infiltrating immune cells. (a, d) Given is the number of infiltrating CD3<sup>+</sup>CD4<sup>+</sup> T helper cells, CD3<sup>+</sup>CD8<sup>+</sup> cytotoxic T cells and IRF5<sup>+</sup> macrophages counted in 2–3 HPFs/slide with n = 3–10 mice/group. (b, c) The infiltration pattern was semi-quantitatively analyzed using a scoring system. 0 = no; 1 = mild; 2 = moderate; 3 = strong. Each symbol represents one case. \**p* < .05; \*\**p* < .01, Two-way ANOVA (Tukey's multiple comparisons test).

the numbers of Tregs and CTLA-4<sup>+</sup> T cells (figure 4f), which is additionally illustrated as tSNE plot in Figure 4g,h Every dot represents one cell. Cells with similar surface markers are located next to each other. In the left upper part of the plot

the Tregs are highlighted. As expected, they are all located very close in one cluster. Larger distances might be due to other expressed surface markers, which were not relevant for our gating of Tregs.



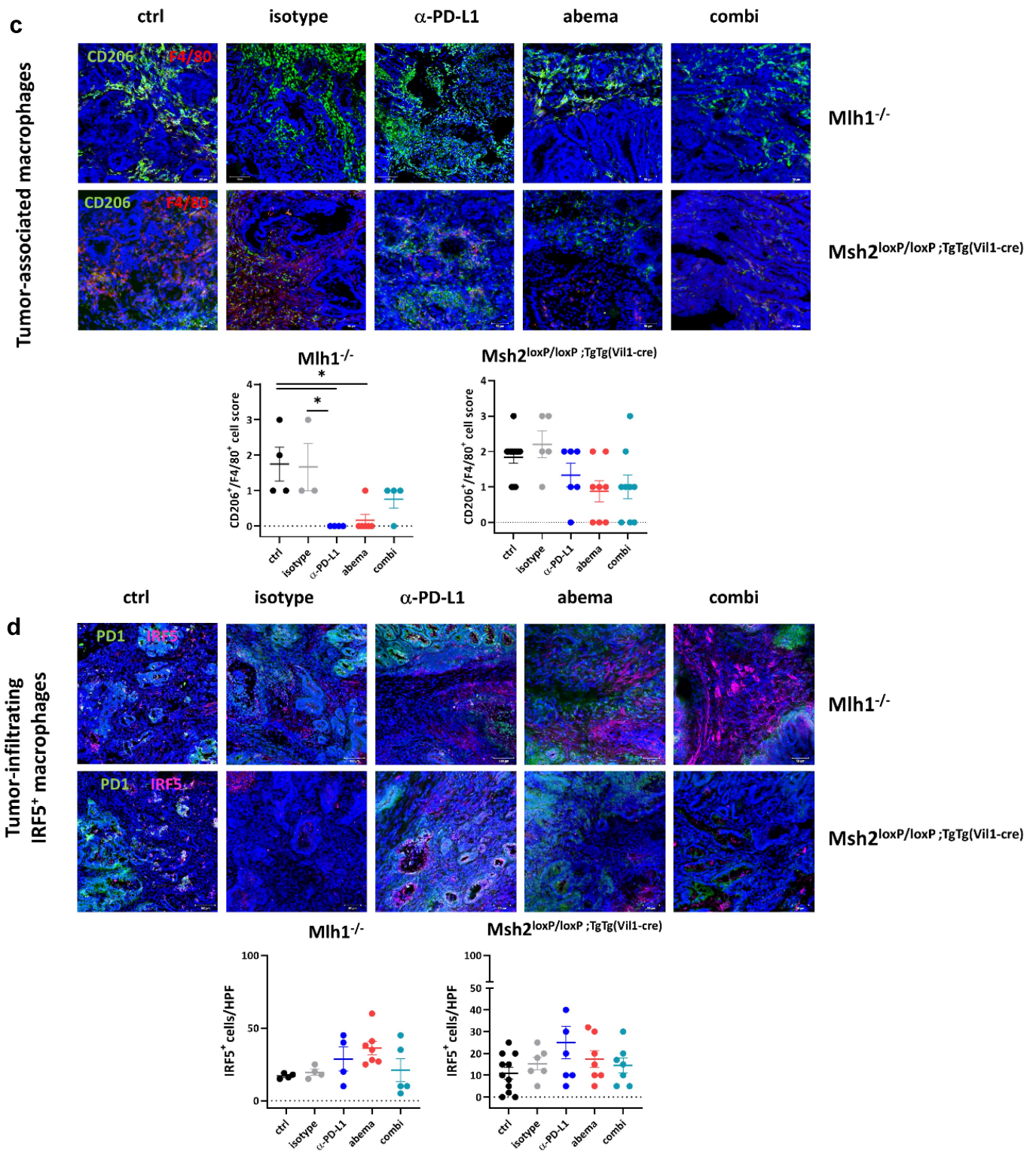


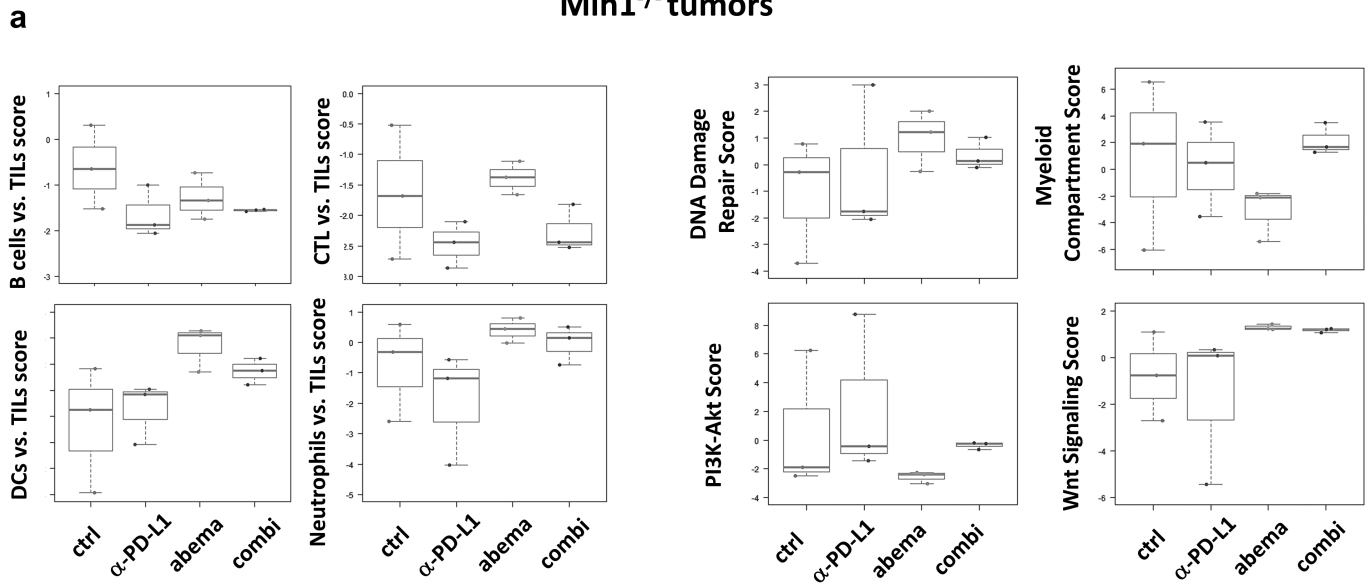
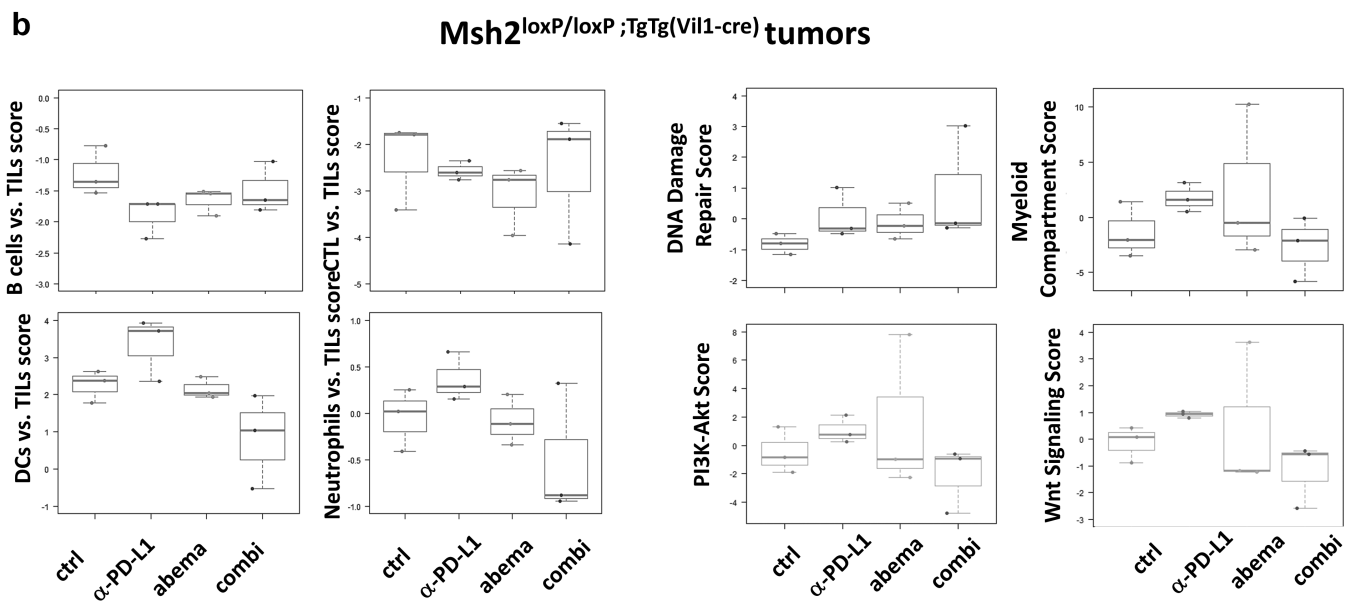
Figure 5. (Continued)

### Treatment-related changes in the tumor microenvironment

The individual effects of either treatment on circulating immune cells were then studied in the local tumor microenvironment. Here, we quantified infiltrating T cells, regulatory CD11b<sup>+</sup>Gr1<sup>+</sup>PD-L1<sup>+</sup> granulocytes, tumor-associated macrophages (TAMs), and IRF5<sup>+</sup> M1 macrophages (Figure 5).

Abemaciclib and  $\alpha$ -PD-L1 monotherapy triggered focal CD3<sup>+</sup>CD4<sup>+</sup> and CD3<sup>+</sup>CD8<sup>+</sup> T-cell infiltration, especially in  $Mlh1^{-/-}$  mice (Figure 5a). Cytotoxic T cell numbers were even significantly elevated under abemaciclib and  $\alpha$ -PD-L1 monotherapy in  $MLH1^{-/-}$  mice, whereas in the combination treatment, this massive immune stimulation was partially abrogated (Figure 5a). In  $Msh2^{loxP/loxP};TgTg(Vil1-cre)$  mice, infiltrating T cell numbers increased upon treatment (Figure 5a). The



**Mlh1<sup>-/-</sup> tumors****Msh2<sup>loxP/loxP</sup>;TgTg(Vil1-cre) tumors**

**Figure 6. Nanostring gene expression analysis of tumors from *Mlh1*<sup>-/-</sup> and *Msh2*<sup>loxP/loxP</sup>;TgTg(Vil1-cre) mice.** The PanCancer IO 360 Gene Expression Panel was applied. Relative abundances measuring various contrasts between cell types reported for each group. Data result from n = 3 samples/group.

overall higher infiltration with T cells was accompanied by decreased numbers of regulatory granulocytes and TAMs in both mouse strains (Figure 5b, c). Quite in line, IRF5, which leads to M1 polarization, was more abundant in abemaciclib-treated tumors and additionally slightly higher upon  $\alpha$ -PD-L1 blockade (Figure 5d). This positive immunomodulatory effect was negated almost completely in both mouse strains receiving the combination.

Supplemental flow cytometric assessment of MLH1<sup>-/-</sup> and *Msh2*<sup>loxP/loxP</sup>;TgTg(Vil1-cre) tumors identified decreased numbers of Tregs in the combination groups (supplementary Figure S3).

The amount of CTLA-4<sup>+</sup> T cells increased in tumors of *Mlh1*<sup>-/-</sup> mice upon abemaciclib mono- and combination therapy, but remained unchanged in *Msh2*<sup>loxP/loxP</sup>;TgTg(Vil1-cre) tumors.

To get a detailed overview of the tumor-infiltrating leukocyte (TIL) compartments and identify treatment-related pathway alterations in-depth, the PanCancer IO 360 Gene Expression Panel was applied (Figure 6 and supplementary Figure S4). B cell levels decreased under all therapies in both mouse strains. In *Mlh1*<sup>-/-</sup> mice, abemaciclib increased the level of cytotoxic T cells within the TIL compartment. Dendritic cell (DC) and neutrophil levels were contrary between the two

mouse strains. Abemaciclib mono- and combination therapy increased the level of both cell types in *Mlh1*<sup>-/-</sup> mice, while in *Msh2*<sup>loxP/loxP;TgTg(Vil1-cre)</sup> mice, it was the other way round.

DNA damage repair genes, such as *Rad51*, *MGMT*, and *Exo1* were higher expressed under abemaciclib mono- and combination therapy in both mouse lines (Figure 6). A comparable effect was seen on *Wnt* signaling, which was highly activated in these two treatment groups, especially in *Mlh1*<sup>-/-</sup> mice. *Vice versa*, the myeloid compartment score as well as genes related to PI3K/Akt or Jak/STAT signaling were reduced (Figure 6, and supplementary Figure S4). Additionally altered genes included those involved in epigenetic regulation and hypoxia. Here again, *Mlh1*<sup>-/-</sup> and *Msh2*<sup>loxP/loxP;TgTg(Vil1-cre)</sup> mice responded contrarily (supplementary Figure S4A,C). In the combination, these strong immune-modulatory effects were almost completely neutralized as illustrated in a heatmap (supplementary Figure S4B, D). Here, the contradictory effects of both monotherapies (abemaciclib,  $\alpha$ -PD-L1) on cellular pathways are shown. In *Mlh1*<sup>-/-</sup> mice, abemaciclib led to

a significant downregulation of most pathways (depicted in blue), but the  $\alpha$ -PD-L1 antibody activated them (depicted in red). In the combination, these opposite effects were blunted. In *Msh2*<sup>loxP/loxP;TgTg(Vil1-cre)</sup> mice, the differences were weaker, still, a comparable trend was seen for most pathway alterations, providing a likely explanation for the missing benefit *in vivo*.

### Treatment-associated gene expression changes in the tumor microenvironment and spleen

The above findings indicated *Wnt* activation by abemaciclib as well as epigenetic modulation by either treatment. Since these mechanisms are drivers of epithelial-mesenchymal transition (EMT), we determined whether this may also play a role here and provide another explanation for the different treatment responses seen under mono- and combination therapy. Therefore, the expression levels of the EMT markers *Tgfb1*, *Vimentin*, *N-Cadherin*, and *Fpr2* were studied by qPCR (Figure 7).

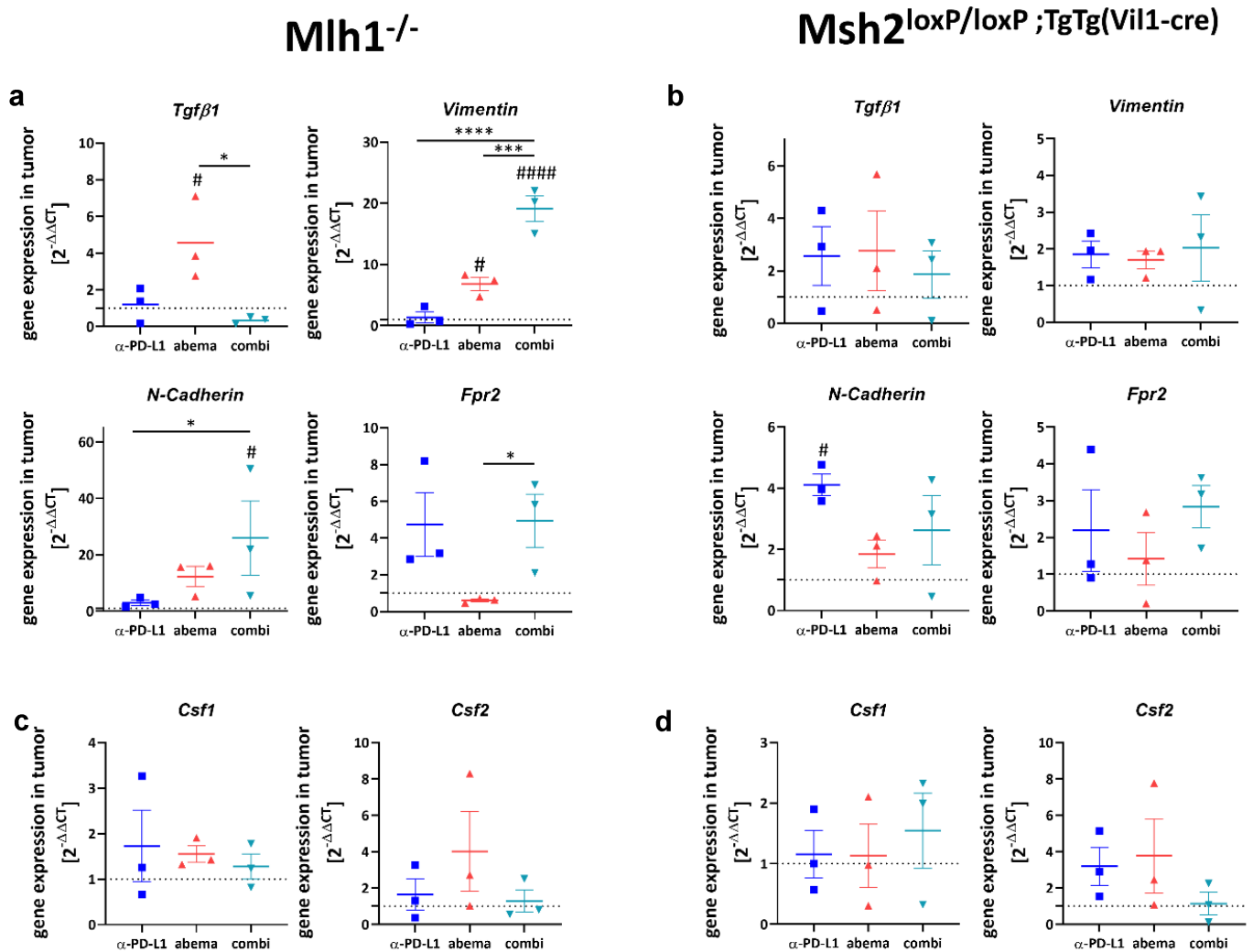


**Figure 7. Expression levels of selected genes and functional immunological analysis.** (a-f) Total RNA from tumors (A-F) and spleens (g, h) was reverse transcribed into cDNA and qPCR was done as described in material and methods. All data are given as  $2^{-\Delta\Delta CT}$  values + SEM. Analysis was done in triplicates with  $n = 3$  mice/group, respectively, \*  $p < .05$ ; \*\*\*  $p < .001$ ; \*\*\*\*  $p < .0001$ ; #  $p < .05$ ; ##  $p < .01$ ; ####  $p < .0001$  vs. control. One-way ANOVA (Tukey's multiple comparisons test) or Kruskal-Wallis test (Dunn's multiple comparisons test).

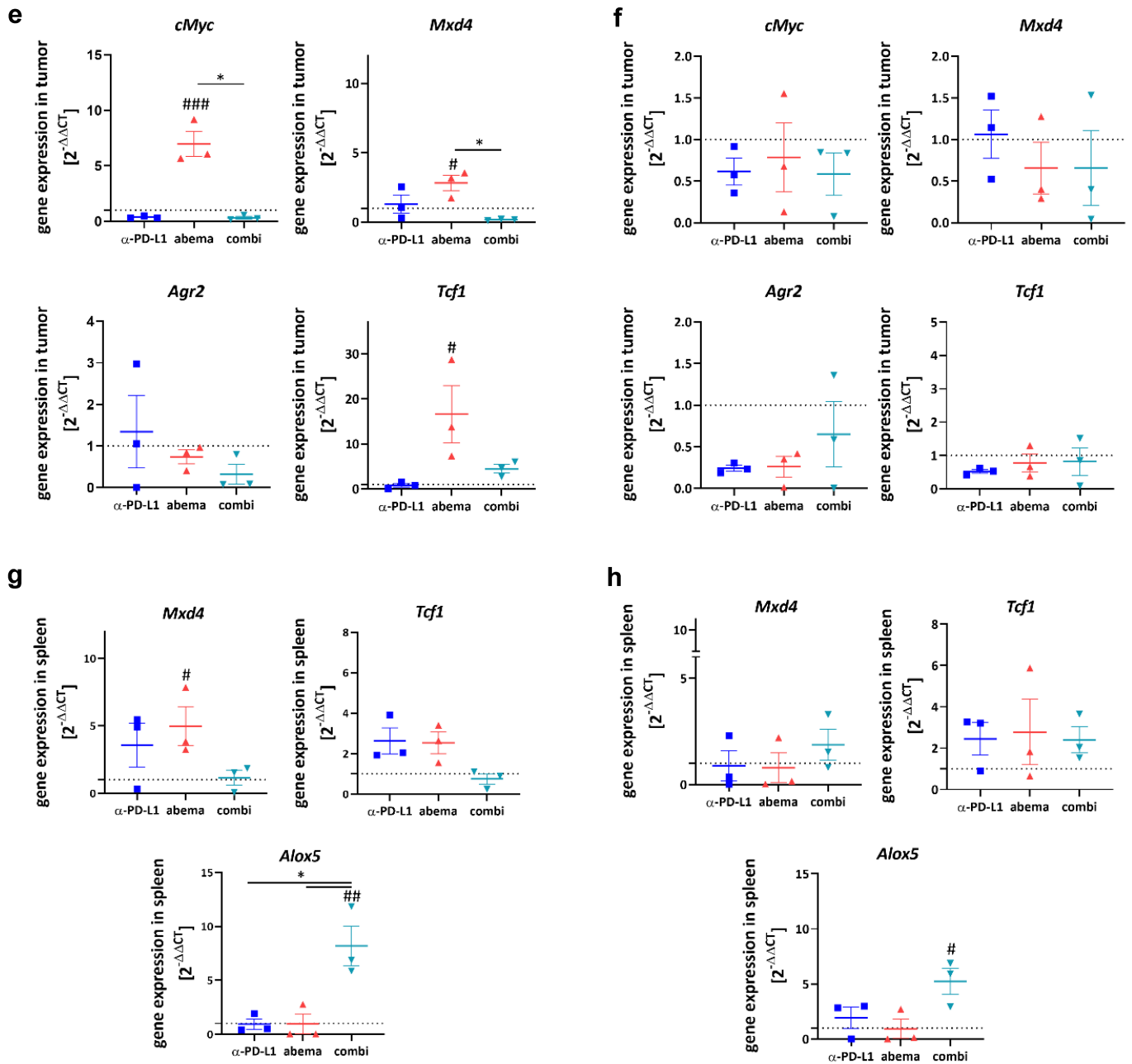
**Mlh1<sup>-/-</sup>****Msh2<sup>loxP/loxP</sup>;TgTg(Vil1-cre)**

Figure 7. (Continued)

Monotherapy with abemaciclib upregulated *Tgfb1*, *Vimentin*, and *N-Cadherin*, but effectively suppressed *Fpr2* in *Mlh1<sup>-/-</sup>* mice (Figure 7a). The α-PD-L1 antibody had no or opposite effects on gene expression. In mice receiving the combination, *Vimentin*, *N-Cadherin*, and *Fpr2* were highly upregulated in residual tumors. The latter is a chemoattractant receptor of G-protein-coupled receptors, which, in conjunction with the EMT effectors *Vimentin* and *N-Cadherin*, triggers cancer invasion.<sup>30</sup>

In *Msh2<sup>loxP/loxP</sup>;TgTg(Vil1-cre)* mice, no such clear correlations were seen. Abemaciclib alone had no impact on EMT markers (Figure 7b). By contrast, α-PD-L1 treatment upregulated *N-Cadherin* and *Fpr2*. Heterogenous effects were seen in the combination group, showing slightly elevated expression levels of *Vimentin*, *N-Cadherin*, and *Fpr2*.

Then, the impact on macrophages was studied (Figure 7c, d). *Csf1* and *Csf2* were used as markers for macrophage polarization. Although statistical significance was not reached, we

observed a trend toward a higher expression of *Csf2* vs. *Csf1* in both mouse strains treated with abemaciclib or  $\alpha$ -PD-L1. *Csf2* is associated with an M1-like phenotype, which supports our above findings on M1-polarization upon monotherapy. Notably, in both mouse models receiving the combination, *Csf1* and *Csf2* were comparable to controls.

Next, we checked genes related to cancer immunity and T cell activation (*cMyc*, *Mxd4*, *Agr2*, *Tcf-1*).<sup>18,31</sup> Abemaciclib induced a significant upregulation of *Myc* and *Mxd4* in *Mlh1*<sup>-/-</sup>, but not *Msh2*<sup>loxP/loxP;TgTg(Vil1-cre)</sup> tumors. Also, *Tcf1*, a transcription factor of the *Wnt* signaling pathway and Treg suppressor,<sup>32</sup> was highly upregulated. *Tcf-1* was recently identified in intratumoral memory CD8<sup>+</sup> T cells with stem cell-like properties.<sup>31</sup> Notably, no such changes were seen upon  $\alpha$ -PD-L1 mono- or combination therapy (Figure 7e). The tumor-promoting anterior gradient-2 (*Agr2*) was found reduced in all mice (*Mlh1*<sup>-/-</sup> and *Msh2*<sup>loxP/loxP;TgTg(Vil1-cre)</sup>) receiving abemaciclib alone or in combination with  $\alpha$ -PD-L1 (figure 7f).

These results prompted us to check for the expression of immunologically and functionally relevant genes in the spleen (Figure 7g, h). Abemaciclib, but not the other treatment regimens, induced *Mxd4* and *Tcf1* in spleens of *Mlh1*<sup>-/-</sup> mice. As anticipated, no significant alterations were detectable in *Msh2*<sup>loxP/loxP;TgTg(Vil1-cre)</sup> mice in either treatment. By contrast, *Alox5*, a neutrophil and macrophage marker with pro-inflammatory and tumor-promoting activity,<sup>33</sup> was highly elevated in both mouse lines receiving the combination.

Finally, mutations in dMMR-specific target genes were examined (supplementary Figure S5). The overall mutation frequency in the tumor compared to normal tissue was slightly elevated under abemaciclib therapy in *Mlh1*<sup>-/-</sup> mice (supplementary Figure S5). In addition, abemaciclib was the only treatment that led to mutations in *Mdm2* and *Ncapd2* and also in combination therapy to mutations in *Spen* and *FAS*. For *Taf1b*, *Kcnma1*, and *Rfc3* nearly all treatments triggered mutations. In *Msh2*<sup>loxP/loxP;TgTg(Vil1-cre)</sup> mice,  $\alpha$ -PD-L1 mono- and combination therapy led to slightly decreased mutation frequency, whereas for the displayed genes, all treatments induced mutations.

## Discussion

Using two clinically relevant mouse models of spontaneous dMMR-driven tumorigenesis, we report that low-dose abemaciclib treatment is as effective as immune-checkpoint blockade, while the combination is not superior to either monotherapy.

Abemaciclib is approved for high-risk early and advanced/metastatic breast cancer.<sup>34</sup> The underlying mode of action includes decreased cell proliferation and induction of senescence.<sup>13,35,36</sup> Here, we also found increased numbers of apoptotic and necrotic cells, a G1-arrest, and impaired colony formation abilities of murine dMMR tumor cells. The latter effect was evident after several days of treatment rest, which is in line with abemaciclib's ability to suppress DNA synthesis even after drug removal.<sup>13</sup> In a co-culture system of *Mlh1*<sup>-/-</sup> tumor and semi-autologous immune cells, abemaciclib boosted cytotoxic effects to an amount much higher than the

therapeutic  $\alpha$ -PD-L1 antibody. Hence, we confirm the strong immune-stimulating potential of this CDKI.<sup>14,15,37</sup> This finding may expand the spectrum of tumors eligible for CDK inhibition.<sup>38</sup>

In a proof-of-concept *in vivo* trial, abemaciclib was given therapeutically to tumor-bearing *Mlh1*<sup>-/-</sup> and *Msh2*<sup>loxP/loxP;TgTg(Vil1-cre)</sup> mice. While both mouse strains responded to CDK4/6 inhibition, disease control was better in the former. Notably, 80% of mice underwent partial remission, finally resulting in significantly prolonged overall survival. In *Msh2*<sup>loxP/loxP;TgTg(Vil1-cre)</sup> mice, the overall survival was similarly extended, but longitudinal PET/CT imaging yielded heterogeneous effects on tumor sizes. The survival benefit was comparable to PD-L1 blockade, which improved the outcome by several weeks. Noteworthy, in this context, is the fact that treatment was given once a week as opposed to most preclinical studies in which a daily treatment regimen is applied.<sup>12,36,37,39</sup> The rationale for this dose reduction is based on the fact that dMMR tumors are highly immunogenic *per se* and pre-formed immune responses may exist.<sup>19,20,40</sup> Accordingly, the primary aim was to re-activate the immune system rather than inducing *de novo* T cell immune responses.<sup>14,16,18,29</sup> With this reduced dosing schedule, abemaciclib still triggered immune modulation, characterized by enhanced secretion of Th1 and Th2-specific cytokines. This was accompanied by reduced numbers of circulating, and to some degree also splenic, CD4<sup>+</sup>CD25<sup>+</sup>FOXP3<sup>+</sup> regulatory T cells – likely due to the CDKI-mediated repression of DNA methyltransferase 1<sup>15</sup>. Tregs express CDK6 at higher levels than effector T cells, making them more vulnerable to CDK inhibition.<sup>15,41</sup> This fact explains why abemaciclib does not impair effector T cell functions. Although these immunological changes emerged in both models, we identified striking differences in the response profile between *Mlh1*<sup>-/-</sup> and *Msh2*<sup>loxP/loxP;TgTg(Vil1-cre)</sup> mice. Given the fact that both strains develop dMMR-related tumors in the gastrointestinal tract (jejunum) spontaneously, this finding is intriguing. However, the mutational driver (*Mlh1* vs. *Msh2*) and the resulting tumor microenvironment (T cells vs. TAMs vs. MDSCs vs. PD-L1 positivity) varies. This is consistent with the human counterpart, e.g. in the tumor mutational burden.<sup>42</sup>

Recent studies describe the restoration of the T cell function by CDK4/6 blockade.<sup>15,18,37,38,43</sup> By dissecting the local immune response in detail, we found significantly increased numbers of cytotoxic T cells and DCs within the TIL compartment, especially in *Mlh1*<sup>-/-</sup> mice. *Vice versa*, numbers of TAMs decreased, accompanied by rising numbers of IRF5<sup>+</sup> cells, reduced levels of the myeloid compartment as well as genes related to PI3K/Akt signaling. Higher expression of IRF5 leads to M1 polarization and the formation of a pro-inflammatory, antitumoral phenotype.<sup>44</sup> Comparable positive immunomodulating side-effects were recently reported for dinaciclib, turning the microenvironment of immunologically 'cold' pancreatic cancers into a 'hot' one.<sup>45</sup> Yet, the plasticity of macrophages may result in dual activation or a mixed M1/M2-like phenotype<sup>46</sup> as seen here upon abemaciclib treatment via upregulation of *CSF1* and *CSF2*. The latter supports the differentiation of hematopoietic myeloid cells<sup>47</sup> and plays an important role in macrophage polarization by enhancing antigen



presentation and DC formation.<sup>48</sup> Here, abemaciclib-treated *Mlh1*<sup>-/-</sup> tumors had elevated numbers of DCs, likely because of CSF2-driven M1 polarization. In the combination, the beneficial effects of the monotherapies were blunted by suppressing activated pathways. Such striking differences in specific subpopulations were primarily detectable in tumors from *Mlh1*<sup>-/-</sup> mice, while *Msh2*<sup>loxP/loxP;TgTg(Vil1-cre)</sup> mice responded differently and effects were often weaker. The exact underlying reason for this model-individual response is not known. A recent study classified inherited and sporadic human dMMR endometrial tumors into distinct immunological entities.<sup>49</sup> Apart from this, dMMR-related malignancies are often grouped together and responses compared to proficient MMR-tumors, without MMR-subclassification, *i.e.* *MLH1*, *MSH2*, *MSH6*, or *PMS2*.<sup>50</sup> Hence, we can only speculate on the cause for the different responses seen here, such as: (I) these two dMMR models were created by different methods (Cre-lox System *vs.* constitutional knock out), the impact of either method on antitumoral immune function is inestimable; (II) *Msh2*<sup>loxP/loxP;TgTg(Vil1-cre)</sup> mice are bred homozygous, while *Mlh1*<sup>-/-</sup> mice are offsprings of heterozygous littermates; (III) the mutational load within coding microsatellites and the loci affected by a specific mutation within tumors differs; and (IV) the tumor microenvironment is heterogeneous.

When looking at regulatory granulocytes, another immune-suppressive subpopulation, only marginal changes were seen. Likewise, circulating and splenic MDSCs increased during after-care and may eventually have contributed to relapse. In support of this, gene expression analysis identified higher amounts of neutrophils within *MLH1*<sup>-/-</sup> and *Msh2*<sup>loxP/loxP;TgTg(Vil1-cre)</sup> tumors, together with high levels of DNA damage repair genes as part of the global stress-response. Another interesting finding of our preclinical *in vivo* trial is the activation of the *Wnt* pathway, which was again higher in *MLH1*<sup>-/-</sup> mice. This effect has been described before as a result of GSK3 $\beta$  inhibition by abemaciclib.<sup>51</sup> GSK3 $\beta$  is an integral kinase within the  $\beta$ -catenin destruction complex. Its specific inhibition by abemaciclib does not apply to other CDK4/6 inhibitors and prospective studies will have to show whether *WNT*/ $\beta$ -catenin activation constitutes a potentially harmful side effect. One of the conceivable effector mechanisms is the induction of epithelial-mesenchymal transformation (EMT), characterized by invasion and enhanced motility.<sup>52</sup> Indeed, abemaciclib triggered *vimentin* and *N-cadherin* expression, especially in *Mlh1*<sup>-/-</sup> mice, but effectively suppressed *Fpr2*, which is also involved in invasion and metastasis.<sup>53,54</sup> We, therefore, conclude a compensatory mechanism to counteract abemaciclib-driven EMT. In the combination, no such “protective” effects were seen, with expression levels of EMT-markers being equal to or higher than in either monotherapy. Therefore, we propose EMT-driven tumor progression as one of the mechanisms that contribute to treatment failure. This hypothesis is supported by comparable findings in *Msh2*<sup>loxP/loxP;TgTg(Vil1-cre)</sup> mice. Although the effects were weaker, we observed a trend toward a higher expression of EMT markers in the combination group.

Another positive effect of CDK4/6 inhibition was recently described on the transcription factor *Mxd4*, a negative regulator of *MYC*.<sup>18</sup> Interestingly, we also found the upregulation of *Mxd4*

after abemaciclib therapy in tumors and spleens of *Mlh1*<sup>-/-</sup> mice, but in contrast to Heckler *et al.*,<sup>18</sup> we additionally detected higher expression levels of *cMyc*. Furthermore, the previously described formation of CD8<sup>+</sup> effector memory cells<sup>18</sup> was not confirmed by us (*not shown*). Despite effective anti-tumor treatment, we conclude a missing long-term immunity, quite possibly attributable to the low-dose and short-term therapy. The fact that neither tumors nor spleens from *Msh2*<sup>loxP/loxP;TgTg(Vil1-cre)</sup> mice showed any changes in these two genes confirm the better outcome of *Mlh1*<sup>-/-</sup> mice functionally.

Considering the effectiveness of PD-L1 blockade, overall survival was comparable between both mouse strains. *Msh2*<sup>loxP/loxP;TgTg(Vil1-cre)</sup> mice tended to benefit more from ICI, likely because of the higher PD-L1 abundance within the tumor stroma. The immunological effects of PD-L1 blockade can be summarized as follows: ICI-monotherapy triggered IL-6 release in both mouse strains, accompanied by reduced levels of exhausted T cells in the blood and slightly elevated levels of tumor-infiltrating T helper and cytotoxic cells. In the TIL compartment, regulatory granulocytes and TAMs faintly decreased. Tregs were only lower in the circulation of both mouse strains. *Vice versa*, splenic or tumor-infiltrating Treg numbers marginally changed. Although we detected higher expression levels of genes involved in antigen presentation, apoptosis, and interferon signaling in tumors of *Msh2*<sup>loxP/loxP;TgTg(Vil1-cre)</sup> mice, the overall immune stimulation was lower as seen for abemaciclib and the beneficial effects were consistently attenuated in the combination. With regard to EMT, ICIs are thought to have a minor direct impact.<sup>55</sup> This is in line with our findings, in which *N-cadherin* was the only elevated gene after  $\alpha$ -PD-L1 blockade in *Msh2*<sup>loxP/loxP;TgTg(Vil1-cre)</sup> mice. Apart from this, no impact was seen on either marker, suggesting no interference with EMT at least in these models.

Finally, the question remains why the combination failed to surpass the respective monotherapy. Preexisting effector T cell levels and dynamic changes in circulating myeloid cells were previously identified as decisive factors for response to combined CDK4/6-immune-checkpoint inhibition (palbociclib + pembrolizumab) in metastatic breast cancer.<sup>43</sup> Here, we did not see such beneficial effects under combination therapy. Tumor growth control and overall survival were not better than in the respective monotherapy. Immunologically, both mouse strains responded with elevated levels of IL-4 in the plasma. IL-4 activates T helper cells, indicating at least partial maintenance of immune stimulation. In support of this, circulating, splenic, and tumor-infiltrating numbers of exhausted T cells were reduced to a degree comparable to abemaciclib monotherapy. In contrast, *Mlh1*<sup>-/-</sup> tumors had reduced cytotoxic T cell levels, which were replaced by TAMs. The latter may have stimulated EMT, characterized by high *vimentin*, *N-cadherin*, and *Fpr2* expression. In *Msh2*<sup>loxP/loxP;TgTg(Vil1-cre)</sup> mice, overall effects were weaker, still, a comparable trend toward neutralizing beneficial effects of either monotherapy, such as apoptosis, co-stimulation, immune cell adhesion, and migration, was seen. Although this finding is somehow underwhelming, it supports recent findings, in which no significant difference in the anti-tumor response was seen compared with the activity of abemaciclib monotherapy.<sup>29,37</sup> By applying a simultaneous setting, the strong immune-modulatory effects

of abemaciclib are not boosted and in some cases, they are even dismantled. This finding complies with results from the phase Ia/Ib PACT study in which patients with advanced, refractory solid tumors received an  $\alpha$ -PD-L1 inhibitor as monotherapy or in combination with abemaciclib.<sup>56</sup> Lead-in CDK inhibition was not feasible due to hepatotoxicity.<sup>56</sup> Detailed immunological analyses were not done in this clinical trial leaving the impact on the immune system unanswered.

To the best of our knowledge, this is the first comprehensive preclinical study reporting the immune-modulatory and therapeutic activity of abemaciclib on dMMR tumors. We not only provide another piece of evidence for the broad entity-overlapping potential of this selective CDKI but additionally propose an interesting option for dMMR patients not eligible for ICI treatment. However, caution is given when abemaciclib is used as lead-in therapy in combination with  $\alpha$ -PD-L1, and follow-up studies are warranted to identify ideal combination partners for CDKI as an immunotherapy backbone.

## List of abbreviations

abema – abemaciclib  
 cMS – coding microsatellite  
 combi – combination  
 ctrl – control  
 dina – dinaciclib  
 dMMR – Mismatch repair-deficient  
 ICI – immune checkpoint inhibitors  
 MDSC – myeloid-derived suppressor cell  
 ROS – reactive oxygen species  
 TAM – tumor-associated macrophages  
 Treg – regulatory T cells

## Acknowledgments

We gratefully thank Genentech, a subsidiary of Roche, South San Francisco, USA, for providing the clone 6E11 for *in vivo* experiments. We additionally thank Mrs. Ilona Klammfuss and Ms. Chantal von Hoersten for breeding mice, Brigitte Vollmar and Bernd Krause for their continuous support in their efforts of chairing the Core Facility of Multimodal Small Animal Imaging. We also gratefully acknowledge the excellent technical assistance of Mrs. Joanna Förster. Furthermore, we thank Carina Bergner and Anja Gummeson, radiopharmacy team of the Department of Nuclear Medicine of the University Medical Centre Rostock, for providing <sup>18</sup>F-FDG for the small animal PET/CT experiments. We likewise thank the Core Facility for Cell Sorting & Cell Analysis, Laboratory for Clinical Immunology, University Medical Center Rostock (Mrs. Wendy Bergmann, Prof. Brigitte Müller-Hilke) for their continuous support and providing access to the technical devices. Moreover, we thank Prof. Winfried Edelmann and Prof. Christoph Gasche for providing Msh2<sup>loxP/loxP;TgTg(Vil1-cre)</sup> breeding pairs and giving the permission to breed mice in our facility.

## Authors' contributions

IS – performed *in vivo* experiments, flow cytometry, analyzed data and participated in writing, LE, JH and PK – performed *ex vivo* analyses (staining of blood, spleen, and tumor samples, immunofluorescence, fragment length), BS – analyzed fragment length analyses; CR – performed Nanostring analysis, HL – provided assistance in confocal laser scanning microscopy, LH and CJ – critically revised the manuscript, CM – conducted the study and applied for grants, participated in the experiments, analyzed data, and wrote the manuscript.

## Disclosure statement

No potential conflict of interest was reported by the authors.

## Ethics approval and consent to participate

The German local authority approved all animal experiments: Landesamt für Landwirtschaft, Lebensmittelsicherheit und Fischerei Mecklenburg-Vorpommern (7221.3-1-062/19; –025/20), under the German animal protection law and the EU Guideline 2010/63/EU. All applicable international, national, and/or institutional guidelines for the care and use of animals were followed.

## Data availability statement

All data generated or analyzed during this study are included in this published article [and its supplementary information files].

## Funding

This work was supported by grants from the German research foundation [DFG grant number MA5799/2-1 and MA5799/2-2] and the Brigitte und Dr. Konstanze Wegener-Stiftung N/A to C; Deutsche Forschungsgemeinschaft.

## References

- Liu J, Zhang S, Hu Y, Yang Z, Li J, Liu X, Deng L, Wang Y, Zhang X, Jiang T, et al. Targeting PD-1 and Tim-3 pathways to reverse CD8 T-cell exhaustion and enhance *ex vivo* T-cell responses to autologous dendritic/tumor vaccines. *J ImmunoTher.* 2016;39(4):171–180. doi:10.1097/CJI.000000000000122.
- Tan E, Sahin IH. Defining the current role of immune checkpoint inhibitors in the treatment of mismatch repair-deficient/microsatellite stability-high colorectal cancer and shedding light on future approaches. *Expert Rev Gastroenterol Hepatol.* 2021 Feb 4;15(7):735–742. doi:10.1080/17474124.2021.1886077.
- Lemery S, Keegan P, Pazdur R. First FDA approval agnostic of cancer site — when a biomarker defines the indication. *N Engl J Med.* 2017;377(15):1409–1412. doi:10.1056/NEJMp1709968.
- Sousa Linhares A D, Battin C, Jutz S, Leitner J, Hafner C, Tobias J, Wiedermann U, Kundi M, Zlabinger GJ, Grabmeier-Pfistershammer K, et al. Therapeutic PD-L1 antibodies are more effective than PD-1 antibodies in blocking PD-1/PD-L1 signaling. *Sci Reports.* 2019;9(1):1–9. doi:10.1038/s41598-019-47910-1.
- Kim JH, Kim SY, Baek JY, Cha YJ, Ahn JB, Kim HS, Lee K-W, Kim J-W, Kim T-Y, Chang WJ, et al. A phase II study of avelumab monotherapy in patients with mismatch repair-deficient/microsatellite instability-high or *POLE*-Mutated metastatic or unresectable colorectal cancer. *Cancer Res Treat.* 2020 Apr 24. doi:10.4143/crt.2020.218.
- Taieb J, André T, El Hajji F, Barbier E, Toullec C, Kim S, Bouche O, Di Fiore F, Chauvenet M, Perrier H, et al. Avelumab versus standard second line treatment chemotherapy in metastatic colorectal cancer patients with microsatellite instability: the SAMCO-PRODIGE 54 randomised phase II trial. *Dig Liver Dis.* 2020;53(3):318–323. doi:10.1016/j.dld.2020.11.031.
- Salewski I, Henne J, Engster L, Schneider B, Lemcke H, Skorska A, Berlin P, Henze L, Junghans C, Maletzki C. Combined gemcitabine and immune-checkpoint inhibition conquers anti-PD-L1 resistance in low-immunogenic mismatch repair-deficient tumors. *Int J Mol Sci.* 2021;22(11):5990. doi:10.3390/IJMS22115990.
- Salewski I, Kuntoff S, Kuemmel A, Feldtmann R, Felix SB, Henze L, Junghans C, Maletzki C. Combined vaccine-immune-checkpoint inhibition constitutes

- a promising strategy for treatment of dMMR tumors. *Cancer Immunol Immunother.* 2021;70(12):3405–3419. doi:10.1007/s00262-021-02933-4.
9. Sahin IH, Akce M, Alese O, Shaib W, Lesinski GB, El-Rayes B, Wu C. Immune checkpoint inhibitors for the treatment of MSI-H/MMR-D colorectal cancer and a perspective on resistance mechanisms. *Br J Cancer.* 2019;121(10):809–818. doi:10.1038/s41416-019-0599-y.
  10. Goetz MP, Toi M, Campone M, Sohn J, Paluch-Shimon S, Huober J, Park IH, Trédan O, Chen SC, Manso L. MONARCH 3: Abemaciclib As Initial Therapy for Advanced Breast Cancer. *J Clin Oncol.* 2017 Nov 10;35(32): 3638–3646. doi:10.1200/JCO.2017.75.6155.
  11. Hino H, Iriyama N, Kokuba H, Kazama H, Moriya S, Takano N, Hiramoto M, Aizawa S, Miyazawa K. Abemaciclib induces atypical cell death in cancer cells characterized by formation of cytoplasmic vacuoles derived from lysosomes. *Cancer Sci.* 2020;111(6):2132–2145. doi:10.1111/cas.14419.
  12. Naz S, Sowers A, Choudhuri R, Wissler M, Gamson J, Mathias A, Cook JA, Mitchell JB. Abemaciclib, a selective CDK4/6 inhibitor, enhances the radiosensitivity of non-small cell lung cancer in vitro and in vivo. *Clin.Cancer Res.* 2018;24(16):3994–4005. doi:10.1158/1078-0432.CCR-17-3575/73825/AM/ABEMACICLIB-A-SELECTIVE-CDK4-6-INHIBITOR-ENHANCES.
  13. Torres-Guzmán R, Calsina B, Hermoso A, Baquero C, Alvarez B, Amat J, McNulty AM, Gong X, Boehnke K, Du J, et al. Preclinical characterization of abemaciclib in hormone receptor positive breast cancer. *Oncotarget.* 2017;8(41):69493–69507. doi:10.18632/ONCOTARGET.17778.
  14. Zhang QF, Li J, Jiang K, Wang R, Ge JL, Yang H, Liu SJ, Jia LT, Wang L, Chen BL. CDK4/6 inhibition promotes immune infiltration in ovarian cancer and synergizes with PD-1 blockade in a B cell-dependent manner. *Theranostics.* 2020;10(23):10619–10633. doi:10.7150/THNO.44871.
  15. Petroni G, Formenti SC, Chen-Kiang S, Galluzzi L. Immunomodulation by anticancer cell cycle inhibitors. *Nat. Rev. Immunol.* 2020;20(11):669–679. doi:10.1038/S41577-020-0300-Y.
  16. Goel S, Bergholz JS, Zhao JJ. Targeting CDK4 and CDK6 in cancer. *Nat. Rev.* 2022;22(6):356–372. doi:10.1038/S41568-022-00456-3.
  17. Hurvitz SA, Martin M, Press MF, Chan D, Fernandez-Abad M, Petru E, Rostorfer R, Guarneri V, Huang CS, Barriga S, et al. Potent cell-cycle inhibition and upregulation of immune response with abemaciclib and anastrozole in Neomonarch, phase II neoadjuvant study in HR+/HER2- Breast cancer. *Clin Cancer Res.* 2020;26(3):566–580. doi:10.1158/1078-0432.CCR-19-1425.
  18. Heckler M, Ali LR, Clancy-Thompson E, Qiang L, Ventre KS, Lenehan P, Roehle K, Luoma A, Boelaars K, Peters V, et al. Inhibition of CDK4/6 Promotes CD8 T-cell Memory Formation. *Cancer Discov.* 2021;11(10):2564–2581. doi:10.1158/2159-8290.CD-20-1540.
  19. Roudko V, Cimen Bozkus C, Greenbaum B, Lucas A, Samstein R, Bhardwaj N. Lynch syndrome and MSI-H cancers: from mechanisms to “Off-The-Shelf” cancer vaccines. *Front Immunol.* 2021;12. doi:10.3389/FIMMU.2021.757804.
  20. Schwitalle Y, Kloor M, Eiermann S, Linnebacher M, Kienle P, Knaebel HP, Tariverdian M, Benner A, Doeberitz MVONK. BASIC – ALIMENTARY TRACT immune response against frameshift-induced neopeptides in HNPCC patients and healthy HNPCC mutation carriers. *Gastroenterology.* 2008;134(4):988–997. doi:10.1053/j.gastro.2008.01.015.
  21. Kloor M, Von Knebel Doeberitz M. The immune biology of microsatellite-unstable cancer. *Trends in Cancer.* 2016;2(3):121–133. doi:10.1016/j.trecan.2016.02.004.
  22. Kortüm B, Campregher C, Lang M, Khare V, Pinter M, Evstatiev R, Schmid G, Mittlböck M, Scharl T, Kucherlapati MH, et al. Mesalazine and thymoquinone attenuate intestinal tumour development in Msh2loxP/loxP Villin-Cre mice. *Gut.* 2015;64(12):1905–1912. doi:10.1136/gutjnl-2014-307663.
  23. Kucherlapati MH, Lee K, Nguyen AA, Clark AB, Hou HJ, Rosulek A, Li H, Yang K, Fan K, Lipkin M, et al. An Msh2 conditional knockout mouse for studying intestinal cancer and testing anticancer agents. *Gastroenterology.* 2010;138(3):993–1002.e1. doi:10.1053/j.gastro.2009.11.009.
  24. Edelmann W, Yang K, Kuraguchi M, Heyer J, Lia M, Kneitz B, Fan K, Brown AMC, Lipkin M, Kucherlapati R. Tumorigenesis in Mlh1 and Mlh1/Apc1638N Mutant Mice. *Cancer Res.* 1999;59:1301–1307.
  25. Maletzki C, Beyrich F, Hühns M, Klar E, Linnebacher M. The mutational profile and infiltration pattern of murine MLH1-/- tumors: concurrences, disparities and cell line establishment for functional analysis. *Oncotarget.* 2016;7(33):53583–53598. doi:10.18632/oncotarget.10677.
  26. Gladbach YS, Wiegele L, Hamed M, Merckenschläger AM, Fuellen G, Junghans C, Maletzki C. Unraveling the heterogeneous mutational signature of spontaneously developing tumors in MLH1 -/- Mice. *Cancers (Basel).* 2019;11(10):1485. doi:10.3390/CANCERS11101485.
  27. Maletzki C, Huehns M, Bauer I, Ripperger T, Mork MMMM, Vilar E, Klöcking S, Zettl H, Prall F, Linnebacher M. Frameshift mutational target gene analysis identifies similarities and differences in constitutional mismatch repair-deficiency and Lynch syndrome. *Mol Carcinog.* 2017;56(7):1753–1764. doi:10.1002/mc.22632.
  28. Lee K, Tosti E, Edelmann W. Mouse models of DNA mismatch repair in cancer research. *DNA Repair (Amst).* 2015;1–7. doi:10.1016/j.dnarep.2015.11.015.
  29. Goel S, DeCristo MJ, Watt AC, BrinJones H, Sceneay J, Li BB, Khan N, Ubellacker JM, Xie S, Metzger-Filho O, et al. CDK4/6 inhibition triggers anti-tumour immunity. *Nature.* 2017;548(7668):471–475. doi:10.1038/nature23465.
  30. Usman S, Waseem NH, Nguyen TKN, Mohsin S, Jamal A, Teh MT, Waseem A. Vimentin is at the heart of epithelial mesenchymal transition (EMT) mediated metastasis. *Cancers.* 2021;13(19):4985. doi:10.3390/CANCERS13194985.
  31. Wen S, Lu H, Wang D, Guo J, Dai W, Wang Z. TCF-1 maintains CD8 + T cell stemness in tumor microenvironment. *J Leukoc Biol.* 2021;110(3):585–590. doi:10.1002/JLB.5MR1120-778R.
  32. Zhang J, Lyu T, Cao Y, Feng H. Role of TCF-1 in differentiation, exhaustion, and memory of CD8+ T cells: a review. *FASEB J.* 2021;35(5):e21549. doi:10.1096/FJ.202002566R.
  33. Weigert A, Strack E, Snodgrass RG, Brüne B. mPGES-1 and ALOX5/-15 in tumor-associated macrophages. *Cancer Metastasis Rev.* 2018;37(2):317–334. doi:10.1007/S10555-018-9731-3.
  34. Groenland SL, Martínez-Chávez A, van DongenMGJ, Beijnen JH, Schinkel AH, Huitema ADR, Steeghs N, van Dongen MGJ. Clinical pharmacokinetics and pharmacodynamics of the cyclin-dependent Kinase 4 and 6 inhibitors palbociclib, ribociclib, and abemaciclib. *Clin Pharmacokinet.* 2020;59(12):1501–1520. doi:10.1007/s40262-020-00930-x.
  35. Klein ME, Kovatcheva M, Davis LE, Tap WD, Koff A. CDK4/6 inhibitors: the mechanism of action may not be as simple as once thought. *Cancer Cell.* 2018;34(1):9. doi:10.1016/J.CCELL.2018.03.023.
  36. Knudsen ES, Hutcheson J, Vail P, Witkiewicz AK, Knudsen ES, Hutcheson J, Vail P, Witkiewicz AK. Biological specificity of CDK4/6 inhibitors: dose response relationship, in vivo signaling, and composite response signature. *Oncotarget.* 2017;8(27):43678–43691. doi:10.18632/ONCOTARGET.18435.
  37. Schaer DA, Beckmann RP, Dempsey JA, Huber L, Forest A, Amaladas N, Li Y, Wang YC, Rasmussen ER, Chin D, et al. The CDK4/6 inhibitor abemaciclib induces a T cell inflamed tumor microenvironment and enhances the efficacy of PD-L1 checkpoint blockade. *Cell Rep.* 2018;22(11):2809–2817. doi:10.1016/j.celrep.2018.02.053.
  38. Lelliott EJ, Sheppard KE, McArthur GA. Harnessing the immunotherapeutic potential of CDK4/6 inhibitors in melanoma: is timing everything? *NPJ Precis Oncol.* 2022;6(1):26. doi:10.1038/S41698-022-00273-9.

39. Dowless M, Lowery CD, Shackelford T, Renschler M, Stephens J, Flack R, Blosser W, Gupta S, Stewart J, Webster Y, et al. Abemaciclib is active in preclinical models of ewing sarcoma via multipronged regulation of cell cycle, DNA methylation, and interferon pathway signaling. *Clin Cancer Res.* 2018;24(23):6028–6039. doi:10.1158/1078-0432.CCR-18-1256.
40. Schwitalle Y, Linnebacher M, Ripberger E, Gebert J, von Knebel Doeberitz M. Immunogenic peptides generated by frameshift mutations in DNA mismatch repair-deficient cancer cells. *Cancer Immunol.* 2004;4:14.
41. Rowell EA, Wang L, Chunder N, Hancock WW, Wells AD. Regulation of T cell differentiation and alloimmunity by the cyclin-dependent kinase inhibitor p18ink4c. *PLoS One.* 2014;9(3). doi:10.1371/JOURNAL.PONE.0091587.
42. Salem ME, Bodor JN, Puccini A, Xiu J, Goldberg RM, Grothey A, Korn WM, Shields AF, Worilow WM, Kim ES, et al. Relationship between MLH1, PMS2, MSH2 and MSH6 gene-specific alterations and tumor mutational burden in 1057 microsatellite instability-high solid tumors. *Int J Cancer.* 2020;147(10):2948–2956. doi:10.1002/ijc.33115.
43. Egelston C, Guo W, Yost S, Lee JS, Rose D, Avalos C, Ye J, Frankel P, Schmolze D, Waisman J, et al. Pre-existing effector T-cell levels and augmented myeloid cell composition denote response to CDK4/6 inhibitor palbociclib and pembrolizumab in hormone receptor-positive metastatic breast cancer. *J Immunother Cancer.* 2021;9(3):e002084. doi:10.1136/JITC-2020-002084.
44. Krausgruber T, Blazek K, Smallie T, Alzabin S, Lockstone H, Sahgal N, Hussell T, Feldmann M, Udalova IA. IRF5 promotes inflammatory macrophage polarization and TH1-TH17 responses. *Nat Immunol.* 2011;12(3):231–238. doi:10.1038/ni.1990.
45. Huang J, Chen P, Liu K, Liu J, Zhou B, Wu R, Peng Q, Liu Z-X, Li C, Kroemer G, et al. CDK1/2/5 inhibition overcomes IFNG-mediated adaptive immune resistance in pancreatic cancer. *Gut.* 2021;70(5):890–899. doi:10.1136/gutjnl-2019-320441.
46. Veremeyko T, Yung AWY, Anthony DC, Strelakova T, Ponomarev ED. Early growth response gene-2 is essential for M1 and M2 macrophage activation and plasticity by modulation of the transcription factor CEBP $\beta$ . *Front Immunol.* 2018;9(NOV):2515. doi:10.3389/FIMMU.2018.02515/BIBTEX.
47. Hercus TR, Thomas D, Guthridge MA, Ekert PG, King-Scott J, Parker MW, Lopez AF. The granulocyte-macrophage colony-stimulating factor receptor: linking its structure to cell signaling and its role in disease. *Blood.* 2009;114(7):1289–1298. doi:10.1182/BLOOD-2008-12-164004.
48. Cai H, Zhang Y, Wang J, Gu J. Defects in macrophage reprogramming in cancer therapy: the negative impact of PD-L1/PD-1. *Front Immunol.* 2021;12. doi:10.3389/FIMMU.2021.690869.
49. Ramchander NC, Ryan NAJ, Walker TDJ, Harries L, Bolton J, Bosse T, Evans DG, Crosbie EJ. Distinct immunological landscapes characterize inherited and sporadic mismatch repair deficient endometrial cancer. *Front Immunol.* 2020;11:10. doi:10.3389/FIMMU.2019.03023.
50. Willvonseder B, Stögbauer F, Steiger K, Jesinghaus M, Kuhn PH, Brambs C, Engel J, Bronger H, Schmidt GP, Haller B, et al. The immunologic tumor microenvironment in endometrioid endometrial cancer in the morphomolecular context: mutual correlations and prognostic impact depending on molecular alterations. *Cancer Immunol Immunother.* 2021;70(6):1679–1689. doi:10.1007/S00262-020-02813-3.
51. Cousins EM, Goldfarb D, Yan F, Roques J, Darr D, Johnson GL, Major MB. Competitive kinase enrichment proteomics reveals that abemaciclib inhibits GSK3 $\beta$  and activates WNT signaling. *Mol Cancer Res.* 2018;16(2):333–344. doi:10.1158/1541-7786.MCR-17-0468.
52. Huang Z, Zhang Z, Zhou C, Liu L, Huang C. Epithelial-mesenchymal transition: the history, regulatory mechanism, and cancer therapeutic opportunities. *MedComm.* 2022;3(2). doi:10.1002/MCO2.144.
53. Lu J, Zhao J, Jia C, Zhou L, Cai Y, Ni J, Ma J, Zheng M, Lu A. FPR2 enhances colorectal cancer progression by promoting EMT process. *Neoplasma.* 2019;66(5):785–791. doi:10.4149/NEO\_2018\_181123N890.
54. Xie X, Yang M, Ding Y, Yu L, Chen J. Formyl peptide receptor 2 expression predicts poor prognosis and promotes invasion and metastasis in epithelial ovarian cancer. *Oncol Rep.* 2017;38(6):3297–3308. doi:10.3892/OR.2017.6034/HTML.
55. Taki M, Abiko K, Ukita M, Murakami R, Yamanoi K, Yamaguchi K, Hamanishi J, Baba T, Matsumura N, Mandai M. Tumor immune microenvironment during epithelial- mesenchymal transition. *Clin Cancer Res.* 2021;27(17):4669–4679. doi:10.1158/1078-0432.CCR-20-4459/672159/AM/TUMOR-IMMUNE-MICROENVIRONMENT-DURING-EPITHELIAL.
56. Patnaik A, Yap TA, Chung HC, de Miguel MJ, Bang Y-J, Lin -C-C, W-C S, Italiano A, Chow KH, Szpurka AM, et al. Safety and clinical activity of a new anti-PD-L1 antibody as monotherapy or combined with targeted therapy in advanced solid tumors: the PACT phase Ia/Ib Trial. *Clin Cancer Res.* 2021;27(5):1267–1277. doi:10.1158/1078-0432.CCR-20-2821.